The legacy of metallurgical atmospheric contamination in a mountainous catchment: A delayed response of Pb contamination

Floriane Guillevic, Fabien Arnaud, Magali Rossi, Jérôme Poulenard, Pierre Sabatier, Anne-Lise Develle, Cécile Quantin, Gaël Monvoisin

The Legacy of Metallurgical Atmospheric Contamination in a Mountainous Catchment: A Delayed Response of Pb Contamination

Floriane Guillevic[1], Fabien Arnaud[1], Magali Rossi[1], Jérôme Poulenard[1], Pierre Sabatier[1], Anne-Lise Develle[1], Cécile Quantin[2], Gaël Monvoisin[2]

[1]Université Savoie Mont-Blanc, CNRS, EDYTEM, F-73000, Chambéry, France

[2]Université Paris-Saclay, CNRS, GEOPS, F-91405, Orsay, France

Keywords: Pb contamination, ore smelting, soil remobilisation, contaminant legacy, Pb inventories

Abstract

Metal-rich fumes emitted during ore smelting contribute to widespread anthropogenic contamination. Environmental archives (such as lake sediments) record fallouts deposited on lake and terrestrial surfaces during ancient mining and smelting activities. However, very few is known about the potential buffering effect of soils upon which metal falls out, prior to be released through runoff and or/erosion, hence leading to pervasive contamination fluxes long after the ceasing of metallurgical activities. Here we aim at assessing this long-term remobilisation in a mountainous catchment area. Lake sediments and soils were collected 7 km upward a 200-year-old historic mine. The Pb-Ag mine of Peisey-Nancroix was operated between the 17th and the 19th centuries with a documented smelting period of 80 years. In lake sediments, the total Pb content varies from 29 mg.kg^{-1} prior smelting to 148 mg.kg^{-1} during ore smelting. Pb isotopes in lake sediments and soils provide evidence of anthropogenic Pb from the local ore (^{206}Pb/^{207}Pb = 1.173; ^{208}Pb/^{206}Pb = 2.094) during and after smelting, suggesting anthropogenic Pb remobilisation for 200 years. The accumulation rates of anthropogenic Pb calculated in lake sediments after the smelting period confirm such a remobilization. Despite a

decrease in this accumulation rate through time, soils still contain significant stocks of anthropogenic Pb (54-89 % of Pb_{ANTH}). The distribution of present-day anthropogenic Pb in the catchment area depends mainly on topographic characteristics. Coupling lake sediments and soils investigations is thus necessary to constrain the long-term persistence and remobilisation of a diffuse contamination related to mining activities.

1. Introduction

The mining industry associated with ore smelting is known to threaten Earth's ecosystems (Hansson et al., 2019; Camizuli et al., 2018; Mariet et al., 2017; Thienpont et al., 2016) through the dispersion of metal-bearing particles into all compartments of the environment (Hong et al., 1994; Renberg et al., 1994; Nriagu and Pacyna, 1988). Numerous studies have investigated the soil contamination in close vicinity of smelting waste storage areas (e.g., Kříbek et al., 2016). However, a substantial amount of metal-bearing particles is also emitted towards the atmosphere during smelting operations. While most of this atmospheric contamination falls out in the vicinity of the smelters (Cloquet et al., 2006; Doucet and Carignan, 2001), a significant fraction of it may spread much further (Brännvall et al., 1997; Hong et al., 1994). One way to track both the spatial distribution and the timing of past pollution is the use of sedimentary archives, such as lake sediments (Arnaud et al., 2004; Corella et al., 2021; Guédron et al., 2016; Sabatier et al., 2014), peatbogs (De Vleeschouwer et al., 2007; Martínez-Cortizas et al., 1999; Shotyk et al., 1998) or ice cores (Hong et al., 1994; Preunkert et al., 2019; Rosman et al., 2000). Environmental archives have been widely used for decades to evidence such a contamination from a regional to a global scale within a long-term perspective (e.g., Mariet et al., 2018). It has been hence shown that global lead contamination occurred as early as during the Antiquity period (Brännvall et al., 2001; Shotyk et al., 1998), while the oldest evidence of metal contamination was dated 4 500 years ago (Leblanc et al., 2000). During the historic period, the Middle Ages was a second major period of widespread metal contamination in Europe

(Brännvall et al., 1999). Since the end of 18th century, industrial mining and smelting has developed, producing large quantities of metal rich-solid wastes and fumes. It has therefore been possible to establish a worldwide history of metal contamination based on environmental archives (Renberg et al., 2001; Shotyk et al., 1998). However, this wide picture does not provide any information about the present-day dispersion and remobilisation within the environment of ancient metal contaminations. Indeed, mining legacy remains of great concern hundreds to thousands of years after activities stoppage (Corella et al., 2021; Le Roux et al., 2020; Hansson et al., 2017; Wiklund et al., 2020), with possible ecotoxicological effects (Camizuli et al., 2018, 2014; Hansson et al., 2019; Monna et al., 2011).

Lake sediments may integrate both direct fallouts and catchment-derived fluxes of contaminating metals. Even when the primary flux has ceased, contaminants stocked in soils can be remobilised by physical erosion and/or runoff waters, and thus enter the recording system (i.e., the lake; Sabatier et al., 2014). Although soil represents the largest reservoir of airborne contaminants (e.g., Pacyna and Pacyna, 2001; Nriagu and Pacyna, 1988), very little is known about the remobilisation of metals after they originally fell out on soils. The storage of trace elements within soil has the potential to act as a secondary source of contamination with a delayed response (Hansson et al., 2019, 2017; Rose et al., 2012; Bacardit and Camarero, 2010; Yang et al., 2002). At the scale of a catchment area, this should induce a time lag between metal fallouts into a catchment and their downstream transfer to a lake basin where they could be stored. However, the lack of data on the duration of ancient mining activities (e.g., Gabrieli and Barbante, 2014) makes it difficult to assess the potential time-lag between metal emission, deposition, remobilisation and finally storage in a given lake catchment area.

The long-term environmental legacy of ancient mining activities is still poorly documented. Remote areas such as high mountain catchments are favourable for studying mining activities far from any urban centre and from other sources of anthropogenic contaminants. This paper

aims to test whether soil erosion contributes to the long-term remobilisation of metals deposited from smelting fumes, in a small valley in the French Alps where mining and smelting occurred between the 17th and the 19th centuries. This study combines geochemical and Pb isotopes analyses of lake sediments and soils from the lake catchment to quantify the amount of anthropogenic lead deposited and its potential remobilisation or storage over 200 years. Anthropogenic Pb accumulation rates and inventories were estimated prior, during and after the smelting period. Finally, these data allow comparing the local anthropogenic Pb flux with the regional flux.

2. Study area

The Peisey-Nancroix Pb-Ag mine is located at 1 500 m a.s.l. in the Ponturin Valley, in the northern French Alps (Savoy; Fig. 1). The first written evidence of ore extraction at the Peisey-Nancroix mine and subsequent smelting on site was dated back to the mid-17th century (1644 CE; Barbier, 1875). However, industrial installations were implemented in the mid-18th century (1734 CE), and the mine was operated until 1866. During this industrial period, 21 500 t of Pb and 53 t of Ag were extracted. For at least 80 years (1745-1824), galena (PbS) and Ag-rich tetrahedrite ($(Cu, Fe)_{12}(Sb,As,Ag)_4S_{13}$) ore was smelted on site, with a great variability in ore production over decades (Table S1; all supplementary tables, text and figures are referenced with an S). For pre-industrial (17th century) and industrial (18th and 19th centuries) times, historical archives written by mining engineers are available. They provide information on the amount of ore extracted and smelted, on the smelting techniques used, and on the spatial distribution of the mining and smelting infrastructures. Ore smelting began to decline in 1813 CE, when smelting facilities were relocated in the city of Albertville (35 km as the crow flies or 65 km down valley from Peisey-Nancroix; Fig. 1B), and was definitively abandoned in 1824 CE. Local contamination of the surrounding hayfields has been engendered by 200-hundred years of mining and smelting waste storage on the surface (Guillevic et al., 2023).

To study atmospheric contaminant emissions during smelting and their subsequent deposition and transfers, Lake La Plagne and its catchment were selected because the lake is located in the upper valley of the Ponturin River, 7 km downwind and upward the former Pb-Ag mining and smelting site (Fig 1C). Lake La Plagne, located at 2100 m a.s.l. in the Vanoise massif, corresponds to a catchment of 1742 ha with a maximum altitude of 3100 m (Fig. 1D). The upper valley is only accessible by foot, and only pastoral activities are known in the area. The bedrock of the catchment consists of metamorphic rocks of the Variscan basement (intermediate to mafic compositions) and carbonate rocks (marble, dolomite, and alpine dedolomitised breccia called "cargneules") from the Mesozoic sedimentary cover (Fig. 1D). A large part of the area is covered by screes and tills. The alpine meadows are covered with *Rumex alpina*, *Nardus stricta, Vaccinium vitis-idea, Achillea millefolium* and *Sempervivum montanum*. The waterways upstream of the 19 m-deep Lake La Plagne cross basement rocks into a peaty-like delta system. The Ponturin River runs from the outlet of the lake northwards before bordering the ancient Pb-Ag mining and smelting site of Peisey-Nancroix, 7 km downstream.

Figure 1 should be inserted here (location map)

3. Materials

3.1 Lake sediments

With the help of a UWITEC gravity corer hammering from a small boat, 5 sediment cores, PLG-01 (IGSN: TOAE0000000343; 1.52 m), PLG-02 (IGSN: TOAE0000000344; 2.25 m), PLG-03 (IGSN: TOAE0000000345; 1.06 m), PLG-04 (IGSN: TOAE0000000347; 0.95 cm), and PLG-05 (IGSN: TOAE0000000349; 2.14 cm), were collected in the centre of Lake La Plagne (N 45°29'2.709''; E 6°50'29.667'', Fig. 1D) in July 2019. Detailed fieldwork information can be found at https://www.cybercarotheque.fr/index.php?mission=PLAGNE. At

the laboratory, each core was split into two halves, one of them was used for the following analyses.

3.2 Surface and subsurface soil samples

A total of 13 surface soil samples were collected with a manual auger at a depth of 0-20 cm along two altitudinal transects in the lake catchment (Fig.1D). Transect A (n = 5) follows a southwestern direction from the west of the lake: samples A1 (2170 m), A2 (2177 m), A3 (2330 m), A4 (2402 m), and A5 (2447 m). Transect B (n = 6) points towards the southeast from the northern side of the lake: samples B1 (2153 m), B2 (2170 m), B3 (2227 m), B4 (2264 m), B5 (2314 m), and B6 (2336 m). Sample B7 (2190 m) was collected between these two transects, and sample B8 (2149 m) was collected in the lake delta. Additionally, two soil profiles were dug at the top of each transect (A5 and B6) to retrieve samples from different soil horizons. Soil samples were air-dried for a few days and sieved to 2 mm before analyses.

4. Methods

4.1. High-resolution elemental EDS-XRF analyses

After visual logging and photographing, the relative major (Al, Si, K, Ca, Mg, Ti, Mn, Fe) and trace (Zn, Pb, As, Rb, Sr, Zr) element contents were measured along the lake sediment core by energy dispersive spectrometer-X-ray fluorescence (EDS-XRF) using the AVAATECH Core scanner at the EDYTEM laboratory. A continuous 1-mm step measurement was performed on a PLG-03 one-half core with multiple runs at 10 kV and 0.2 mA during 15 s, allowing the detection of lightweight elements, and a second run at 30 kV at 0.15 mA during 20 s to detect heavy elements. In order to discriminate As and Pb, which suffer from peak overlap, peak intensities were calculated using only Pb_Lß and As_Ka. Argon was also analysed and used as an element control for the homogeneity of the core. Hierarchical clustering on principal component analysis (PCA) of major elements was applied to compare visual logging to

geochemical units of lake sediment using the multivariate analysis package FactoMineR (Lê et al., 2008) in R statistical software (R Core Team, 2022).

4.2 Carbonates and organic matter content

The determination of the organic matter and carbonate contents of the lake sediments was performed by loss on ignition (LOI) on discrete samples from PLG-03 following the method by Heiri et al. (2001). The weight loss was measured after a first heating step at 550°C (LOI_{550}), providing an assessment of the organic matter content within lake sediments, and after a second heating step at 950°C (LOI_{950}), used as a proxy of the carbonate content.

The carbon total content (inorganic and organic fraction, C_T) of the fine fraction of soils was measured by dry combustion (ISO 10694), and the $CaCO_3$ total content ($CaCO_3$, ISO 10693) was measured by the volumetric method at the French national reference soil laboratory (INRAE, France). Based on the C_T and $CaCO_3$ contents, the total organic carbon (TOC, $TOC = C_T – (0.12 \times CaCO_3)$) and the soil organic matter (OM, $OM = 1.7 \times TOC$) were calculated. The pH of the soil samples was also measured.

4.3 Major and trace element contents, and enrichment factor (EF)

Following the routine analysis of Carignan et al. (2001), soils (< 2 mm; n = 13) and lake sediment samples (n = 66) were analysed for 54 elements after lithium tetraborate fusion using ICP–OES iCap6500 (major elements) and ICP–MS iCapQ (trace elements) at the Service d'Analyse de Roches et Minéraux (SARM-CNRS, Nancy, France). Total concentration uncertainties were about 1% for major elements and between 5% and 10% for trace elements, depending on concentration levels. Reference materials and blanks were prepared along with the samples. Lake sediment sampling along the core was performed approximatively at each cm according to facies changes for a total of 66 samples for a 106cm core (PLG-03). Sampling was spaced to avoid thick instantaneous events identified during logging, such as event deposits

that were considered instantaneous deposits and non-representative of continuous sedimentation (Sabatier et al., 2022; Arnaud et al., 2002). In this paper, major and trace element contents are presented as the median ± standard deviation.

For both soil and lake sediments, the enrichment factor (*EF*) of potentially toxic trace elements (PTEs) was calculated to quantify the PTE contamination in comparison to a reference background:

$$EF_{\mathrm{M_1}} = \frac{(\frac{M_1}{M_2})_{SAMPLE}}{\left(\frac{M_1}{M_2}\right)_{\mathrm{BKG}}} \qquad equation\ (1)$$

where M_1 is the Pb or As content of the sample and of the reference background (BKG), and M_2 is the content of a selected "conservative" element in soil and lake sediments that has exclusively a lithogenic origin (Reimann and de Caritat, 2000) and a content on the same order of magnitude as the studied PTE. Both Rb and Th were tested as conservative lithogenic elements for the calculus of the *EF*. The classification of *EF* is presented in Table S2.

4.4 Pb isotopes

A selection of lake sediment (n = 9) and all soil samples (surface and subsurface horizons, n = 20) were analysed for Pb isotopic composition (^{204}Pb, ^{206}Pb, ^{207}Pb and ^{208}Pb) using a Thermo Fischer Multicollector (MC-ICP–MS) Neptune Plus at the SARM-CNRS laboratory. After digestion, the samples are placed on an ion exchange resin to chemically separate the mineral matrix. Lake sediment samples were chosen before the sampling of the continuous 66 discrete samples based on the Pb and As peaks identified on the EDS-XRF profiles. Two samples (85-86 cm and 103-104 cm) presenting the lowest Pb and As abundances were chosen to define isotopic composition of the local background.

In-situ Pb isotope measurements were performed on 10 to 20 individual galena crystals of two ore-bearing samples collected on the waste heaps to determine the local ore signature. Measurements were performed at the CRPG-CNRS (Nancy, France) using the 1270 ion microprobe in monocollection mode to a mass resolution of 4000, following Deloule et al. (1986).

4.5 Short-lived radionuclides (^{210}Pb, ^{137}Cs, ^{230}Am)

The activities of natural short-lived radionuclides ^{210}Pb, ^{226}Ra and ^{7}Be and artificial radionuclides ^{241}Am and ^{137}Cs in lake sediment samples were measured at the Laboratoire Souterrain de Modane (LSM, France) on EDYTEM-operated low background SAGe well detectors (Reyss et al., 1995). For each sample, the excess ^{210}Pb ($^{210}Pb_{ex}$) activities were calculated as the difference between the total ^{210}Pb and ^{226}Ra activities. The first 30 cm of lake sediments from the PLG-03 core were sampled according to lithological variations, approximatively each cm. Using a small cylinder (3 cm^3), the dry bulk density (DBD) was determined by measuring the dry weight for a constant volume of sediment before analysis. Short-lived radionuclide data were computed with the serac package (Bruel and Sabatier, 2020) in R software (R Core Team, 2022) build an age-depth model for the recent sediments.

4.6 ^{14}C dating

Organic macroremains were sampled for ^{14}C (radiocarbon) dating from cores PLG-01, PLG-03, PLG-04 and PLG-05, which were correlated from visual observation. Despite difficulties in providing a proper quantity of macroremains, 13 samples were dried at 60°C and sent to the accelerator mass spectrometer (AMS) of the Poznan Radiocarbon laboratory (Poland) to measure ^{14}C. The radiocarbon ages were calibrated with the Intcal20 calibration curve (Reimer, 2020) using the clam package (Blaauw, 2010) in R software (R Core Team, 2022) to construct

a single age-depth model correlated with short-lived radionuclide measurements (^{210}Pb, ^{137}Cs, ^{231}Am).

4.7 Anthropogenic Pb (Pb_{ANTH}) and accumulation rate (AR_{Pb_ANTH})

Two methods were used to measure the anthropogenic Pb (Pb_{ANTH}) of lake sediments and soils: elemental and isotopic methods. First, the total Pb content of one sample (Pb_{TOTAL}) is considered as the sum of the lithogenic background Pb (Pb_{BKG}) and the anthropogenic Pb contents; $Pb_{TOTAL} = Pb_{BKG} + Pb_{ANTH}$. To take into account the natural variations related to changes in the terrigenous fraction, the lead concentration was normalized to a conservative lithogenic element that is not emitted into the atmosphere during smelting, following equation (2):

$$Pb_{\mathrm{ANTH}} = Pb_{\mathrm{TOTAL}} - \left(Rb_{\mathrm{TOTAL}}\, x\, \left(\frac{Pb_{\mathrm{BKG}}}{Rb_{\mathrm{BKG}}} \right) \right) \quad equation\ (2)$$

Second, the calculation of Pb_{ANTH} was also determined isotopically using a two end-member mixing model, where the mean of the two deepest lake sediment samples represent the lithogenic background end-member (85-86 cm and 103-104 cm):

$$Pb_{\mathrm{ANTH}} = Pb_{\mathrm{TOTAL}}\, x\, \frac{\left(\frac{Pb^{206}}{Pb^{207}}\right)_{\mathrm{sample}} - \left(\frac{Pb^{206}}{Pb^{207}}\right)_{\mathrm{BKG}}}{\left(\frac{Pb^{206}}{Pb^{207}}\right)_{local\_ore} - \left(\frac{Pb^{206}}{Pb^{207}}\right)_{\mathrm{BKG}}} \quad equation\ (3)$$

The accumulation rate of anthropogenic Pb (AR_{Pb_ANTH}) represents the annual flux of anthropogenic Pb per m^2. It was calculated in lake sediments to evaluate changes in metal accumulation along the sediment core, and to compare the Lake La Plagne accumulation rate to regional fluxes that were estimated at Lake Anterne (Fig1B) during the same time period. The AR_{Pb_ANTH} (in mg.m^{-2}.y^{-1}) was calculated according to equation (4):

$$AR_{Pb\_\mathrm{ANTH}} = SR\ x\ DBD\ x\ Pb_{\mathrm{ANTH}} \quad equation\ (4)$$

where *SR* is the sedimentation rate (or accumulation rate, in $mm.y^{-1}$) obtained from the age-depth model, *DBD* is the dry bulk density (in $g.cm^{-3}$) and Pb_{ANTH} corresponds to the anthropogenic Pb content (in $mg.kg^{-1}$). Details on the *DBD* calculation of lake sediments and the fine fraction of soil (< 2 mm) are presented in Text S1.

4.8. Inventory calculations

4.8.1 Inventories of anthropogenic Pb ($g.m^{-2}$):

The inventory of anthropogenic Pb ($Inv._{Pb}$) represents the quantity of anthropogenic Pb stored per unit area in soils or in lake sediments (in $g.m^{-2}$). For lake sediments, it is possible to calculate the total amount of metal accumulated for the area of the sediment core ($Inv._{Pb\_lake\_sed}$) following equation (5):

$$Inv._{\text{Pb\_lake\_sed}} = \sum_{i=1}^{n} SR\ x\ DBD\ x\ Pb_{\text{ANTH}} = \sum_{i=1}^{n} AR_{\text{Pb\_ANTH}} \quad equation\ (5)$$

where n is the thickness of the accumulated sediment, which represents a time period using the age-depth model.

For soils, the inventory ($Inv._{Pb\_soil}$) is calculated following equation (6), with *T* being the thickness of the soil to integrate:

$$Inv._{\text{Pb\_soil}} = T\ x\ DBD\ x\ Pb_{\text{ANTH}} \quad equation\ (6)$$

4.8.2 Inventories of $^{210}Pb_{ex}$ ($Bq.m^{-2}$):

The larger the catchment area, the larger the amount of sediment, and therefore the more the anthropogenic contaminant is expected to be remobilised (assuming uniform fall-outs). A focus factor (*FF*) is calculated to compare inventories of $^{210}Pb_{ex}$ (fine sediment proxy) among lakes:

$$FF = \frac{Inv.Pb_{ex}^{210}{}_{\text{PLG}}}{Inv.Pb_{ex}^{210}{}_{\text{ANT}}} \quad equation\ (7)$$

with $Inv.Pb_{ex}^{210}{}_{\mathrm{PLG}}$ the inventory of $^{210}Pb_{ex}$ in Lake La Plagne (PLG), and $Inv.Pb_{ex}^{210}{}_{\mathrm{ANT}}$ the inventory of $^{210}Pb_{ex}$ in Lake Anterne (ANT). A $FF > 1$ indicates a net accumulation of sediment. The FF will allow calculating the difference in anthropogenic Pb accumulated over a given period of time and the local surplus of anthropogenic Pb ($Surplus_{Pb}$ in $g.m^{-2}$) potentially engendered by smelting activities, following equation (8).

$$Surplus_{\mathrm{Pb}} = Inv._{\mathrm{Pb\_PLG}} - FF\ x\ Inv._{\mathrm{Pb\_ANT}} \quad equation\ (8)$$

Lake La Plagne was compared to Lake Anterne (Fig. 1B) as (i) its relatively small catchment area (256 ha) makes it a good atmospheric recorder, and (ii) there was no important metallurgical activity in the 18th and 19th centuries nearby, so that it only recorded the regional atmospheric signal.

5. Results

5.1 Sedimentology of Lake La Plagne

As it is often the case in alpine lakes, many event layers are interbedded with the continuous sedimentation in Lake La Plagne sediment cores. These layers show a coarser grain size at the base (normal grading) associated with few millimetres size organic debris. They present a beige or brown yellowish colour contrasting with the dark brown facies characterising the continuous sedimentation. The correlation between the 5 cores is mainly based on events and is reported in the supplementary material Fig. S1 A list of the event depths is reported in Table S3 for each core studied.

The continuous sedimentation presents slight changes over the studied sequence and was thus divided into 4 units based on XRF logging, LOI_{550} and LOI_{950} data. Unit 1 (6-11 cm; 25- 45 cm, Fig. 2) consists of a dark brown silt with LOI_{550} up to 8 wt. % (5.1 ± 1.9 wt. %), which is slightly higher than for the other units. The carbonate content estimated based on LOI_{950} is also the highest among the continuous sedimentation units (18.0 ± 4.6 wt. %). This

induces a lower DBD (0.8 ± 0.2 $g.cm^{-3}$) than for the more silicate-rich units found at depth (Fig. 2). Only the sediment colour allows distinguishing Unit 2 (45-64 cm) from Unit 3 (78-87 cm; 99.5-107 cm), as their LOI_{550} and LOI_{950} are similar (4.3-4.7 and 9.3-10.6 wt. %, respectively). The slightly lower organic content of Unit 2 (4.3 ± 1.3 wt. %) may be responsible for its greener colour in comparison to the brown-dark colour of Unit 3 (4.7 ± 1.3 wt. %). Unit 4 (87-99.5 cm) corresponds to laminated mixing between Unit 2 and Unit 3.

Figure 2 should be inserted here (lithostratigraphic description of core PLG19-03).

5.2 Major elements

5.2.1 Lake sediments

Three clusters were identified from hierarchical clustering (Fig. S2). The first dimension (50.73 %) and the second dimension (29.18 %) of the PCA distinguish carbonate-rich top event layers (cluster 1) and terrigenous continuous sedimentation (clusters 2 and 3). This classification corroborates the total major element contents (Fig. 2), showing a lower SiO_2 content (22.3 ± 9.3 wt. %, n = 16) and a higher CaO content (19.4 ± 4.1 wt. %) in the carbonate-rich events compared to continuous sedimentation (SiO_2: 39.3 ± 6.4 wt. %; CaO: 7.9 ± 3.3 wt. %, n = 53).

The continuous sedimentation represented by cluster 2 and cluster 3 encompassed the 4 units identified during logging as well as the deep event layers (64-78 cm; 87-91 cm; 93-95 cm and 98-99 cm). These deep events, which have a geochemical signature similar to the continuous sedimentation (Fig. S2), are identified based on their brown-yellowish colour and sandy texture. Unit 2, Unit 3 and Unit 4 present similar major element contents whereas Unit 1 presents a higher carbonate content, thus diluting the silicate signal.

5.2.2 Soils

Most soils from the Lake La Plagne catchment are developed on basement rocks and/or till with minor proportions of carbonate fragments, which are abundant in screes (Fig. 1D). These soils can be classified as rankosols with the exception of sample B8, which is a saturated fluviosoil with the highest $CaCO_{3T}$ content (5 wt. %, Table 1). The other surface soils are silty-sandy soils with no carbonates (< 1 wt. % $CaCO_{3T}$). The total organic carbon (TOC) content varies from 6 to 12 wt. %. Superficial soils collected on basement rocks and tills (A2, A4, B1, B3, B4, B5 and B6) presented a higher SiO_2 content (52.4 ± 4.5 wt. %) and a lower CaO and MgO contents (0.7 ± 0.5 wt. %; and 2.3 ± 0.4 wt. %; respectively) than the soils overlying the cargneules and the carbonate-rich screes (SiO_2: 43.9 ± 3.5 wt. %; CaO: 1.6 ± 2.4 wt. %; MgO: 3.8 ± 1.5 wt. %; A1, A3, A5, B2, B7, B8).

Surface soils have heterogeneous pH values ranging between 4.5 and 7.6 (Table 1). The most alkaline soils (pH > 7; samples A1, B2, B7 and B8) are located down the slope or along the slopes with downhill carbonate rock outcrops. The most acidic soils (pH < 5; samples A2, A4, B4 and B5) are developed on basement rocks of the catchment. Soil samples A3, A5, B1, B3, and B6 present an intermediate pH.

Table 1 should be inserted here (Soil properties and mean major and trace elements)

5.3 Trace elements and enrichment factor

5.3.1 Lake sediments

Among the elements of metallurgic interest, Pb and As show clear variations according to XRF scanning. In contrast, Zn, Cu and Ni display weak and noisy signals. No signal was recorded for Sb despite the presence of Sb-bearing minerals in the ore. The Pb profile shows three peaks (56.5-58.3 cm, 82.5-79.5 cm, and 62.5-64.5 cm) interspersed with event layers (in red, Fig. 2). The As profile shows 2 peaks (30-31 cm and 27.9-29.3 cm) also interspersed with an event layer.

The total trace element contents in discrete samples confirmed that apart from Pb and As, the other potentially toxic trace elements (PTE; Ni, Cu, Sb and Zn) do not display any positive anomaly. The Ni content varied between 12 and 37 $mg.kg^{-1}$ (26.7 ± 4.5 $mg.kg^{-1}$), the Cu content varies between 16 and 51 $mg.kg^{-1}$ (39.3 ± 5.3 $mg.kg^{-1}$), the Zn content varied between 69 and 235 $mg.kg^{-1}$ (182.6 ± 28.5 $mg.kg^{-1}$), and the Sb content varied between 1.8 and 4.1 $mg.kg^{-1}$ (3.0 ± 0.4 $mg.kg^{-1}$). The total arsenic content confirmed the EDS-XRF data, with the As content varying from 34.7 to 505 $mg.kg^{-1}$ (87.8 ± 109.0 $mg.kg^{-1}$). Simultaneously, for the As peaks, an increase in the organic matter was measured with $LOI_{550°C}$ (between 6 and 8 wt. %, Fig. 2).

The total Pb content varies from 29 to 148 $mg.kg^{-1}$ for the continuous sedimentation samples (61.5 ± 30.4 $mg.kg^{-1}$, n = 54). The deepest lake sediment samples (85 to 106 cm) present a low Pb content, between 29 and 38 $mg.kg^{-1}$. The highest Pb content was measured between 54 and 85 cm (from 47 to 148 $mg.kg^{-1}$). This confirmed the 3 Pb peaks identified from the EDS-XRF profile (Fig. 2). From the top of the core to 54 cm, the total Pb content varies between 29 and 87 $mg.kg^{-1}$. The total Pb content of one of the top events (6 to 7 cm) reaches 690 $mg.kg^{-1}$ between 6 and 7 cm (Fig. 2), which is quite surprising considering that no major Pb peak was identified by EDS-XRF at this depth in any core (Fig S3).

The EF_{Pb} was calculated for each lake sediment discrete sample using for reference background the mean Pb/Rb ratio of the discrete samples collected between 85 and 106 cm (Pb/Rb: 0.32 ± 0.02, n = 15), which are considered to represent the local geological background. Element Rb was chosen over Th as the conservative element because its standard error of the mean background ratio was lower and because Rb was identified within the terrigenous fraction (Fig. S2). The enrichment was considered significant for $EF_{Pb} > 2$. Table S4 presents EF_{Pb} values in depth along the sediment core. From 0 to 55 cm, the EF_{Pb} increases from 2 to 4. From 55 to 62 cm, the EF_{Pb} is equal to 3, showing a minor enrichment. From 62 to 81 cm, the EF_{Pb}

shows a moderate enrichment up to 5. As the deeper sediments are used for background and reference values, EF_{Pb} is close to 1 between 85 and 106 cm.

5.3.2 Soils

The Pb content in superficial soil samples varies from 39 to 132 $mg.kg^{-1}$ (96.2 ± 28.2 $mg.kg^{-1}$), with a high variability depending on the sample location, but no relationships with the underlying lithologies (Table 1 and Fig. 3). The deepest soil horizons of profiles A5 (overlying cargneule and dolomite) and B6 (developed on basement-rich tills lying over cargneule and dolomitic rocks) present equivalent Pb/Th ratios. Despite lithological differences, these deepest horizons are used as background references to calculate enrichment factors in soils as their Pb/Th ratios are equivalent (Pb/Th ~ 2.7). EF_{Pb} in soils varies between 2 and 9 (Fig. 3). Despite Pb enrichment, the PTE contents (Ni, Cu, As, Sb) of surface soil samples are very low and therefore show no significant enrichment (Table 1). The depth transfer of Pb is limited; only the first two horizons of profiles A5 and B6 show moderate to severe Pb enrichment whereas the deeper horizons display no enrichment (Table S5).

5.4 Pb stable isotopes

5.4.1 Local ore

The local galena displays $^{206}Pb/^{207}Pb$ ratios of 1.172 ± 0.002 and $^{208}Pb/^{208}Pb$ ratios of 2.095 ± 0.005 (n = 29, Table S6) that will be named Pb local ore in the following.

5.4.2 Lake sediments

The two deepest samples of the lake sediment core present a $^{206}Pb/^{207}Pb$ isotopic ratio of 1.209 and a $^{208}Pb/^{206}Pb$ isotopic ratio between 2.041 and 2.042 (Fig. 4, Table S7), falling within the range of the Variscan continental crust (Monna et al., 2000). Hence, these samples may be considered as the uncontaminated local background. On a $^{206}Pb/^{207}Pb$ vs $^{208}Pb/^{206}Pb$ diagram, the lake sediment Pb isotopic signatures provide evidence of binary mixing between the local

375 background and the local Pb ore end-members (Fig. 4A). The proportion of anthropogenic Pb
376 calculated from $^{206}Pb/^{207}Pb$ (Pb_{ANTH}, equation 3) decreased from 79-84% at 80 cm depth down
377 to 20-25% at the top of the core (Table S8). The anthropogenic Pb in the deeper samples at
378 52 cm, 57.5 cm, 63.5 cm, and 80 cm represents more than 50% of the total Pb content (59%,
379 66%, 79% and 84%, respectively). Such high proportions of Pb_{ANTH} are related to the highest
380 Pb contents (e.g., at 80 cm, Pb = 48 $mg.kg^{-1}$). Even though the shallowest samples (7.3 cm,
381 10 cm and 30.5 cm) only displayed minor enrichment from the EF_{Pb} calculation, their Pb
382 isotope ratios display significant proportions of anthropogenic Pb, of 24%, 43% and 50%,
383 respectively.

384 *5.4.3 Soils*

385 The Pb isotope signature of the soil samples (Table S7) indicates a binary mixing between the
386 local Pb-ore and the geochemical background end-members (Fig. 4), suggesting the persistent
387 presence of anthropogenic Pb derived from local metallurgy. Samples A3, A5, B3 and B7 have
388 isotopic signatures close to or in the range of the local background end-member (between 1.195
389 and 1.209 for $^{206}Pb/^{207}Pb$ and between 2.038 and 2.059 for $^{208}Pb/^{206}Pb$). Samples A2, A1, B6
390 and B1 present isotopic signatures close to the local galena (between 1.177 and 1.180 for
391 $^{206}Pb/^{207}Pb$ and between 2.085 and 2.089 for $^{208}Pb/^{206}Pb$). Samples A4, B8, B4 and B2 have an
392 intermediate isotopic signature between the local Pb ore and the geochemical background end-
393 members (between 1.185 and 1.189 for $^{206}Pb/^{207}Pb$ and between 2.069 and 2.078 for
394 $^{208}Pb/^{206}Pb$). Sample B5 has an isotopic signature similar to the Pb local ore. The subsurface
395 soil samples of profile A5 and the deepest soil horizon of B6 show a more radiogenic signature
396 ($^{206}Pb/^{207}Pb$ ranging from 1.24-1.29) than the local geochemical background (Fig. 4). Such
397 heterogeneity in geogenic signatures made it difficult to calculate the proportion of
398 anthropogenic Pb in soils from the Pb isotope ratios. However, the fraction of the anthropogenic
399 Pb was calculated from isotopic ratios using equation (3) according to the different lithologies

and was compared with the fraction of anthropogenic Pb calculated from the elemental method using equation (2) (Table S8; see discussion).

Figure 4 should be inserted here (Pb isotopes)

5.5 Age-depth model of lake sediments

Applying a constant flux-constant sedimentation rate (CFCS) model to an event-free sedimentary sequence (Bruel and Sabatier, 2020), the $^{210}Pb_{ex}$ activity profile indicates two distinct periods of constant accumulation rate (AR; Fig. 5): i) AR = 0.99 ± 0.3 mm.y^{-1} between 0 and 245 mm, and ii) AR = 1.25 ± 0.2 mm.y^{-1} between 245 and 335 mm. According to the computed age-depth model, the change in sedimentation rate occurred in 1982 ± 10 y. The downcore ^{137}Cs activity profile shows a first small peak at a depth of 104 ± 10 mm and a second peak at 290 ± 10 mm, which are associated with a peak in ^{241}Am activity. The uppermost peak is attributed to the Chernobyl accident in 1986 CE and is in relatively good agreement with $^{210}Pb_{ex}$ derived ages (Fig. 5 on the right, Appleby et al., 1991). However, the $^{210}Pb_{ex}$ derived ages are poorly equivalent to the deepest and maximum nuclear test fallout in 1963 CE, identified from both ^{137}Cs and ^{241}Am activity peaks. Therefore, ^{137}Cs and ^{241}Am peaks were used as privileged time-markers for the age-depth model combining ^{14}C dates (Smith, 2001).

Figure 5 should be inserted here ($^{210}Pb_{ex}$ ^{137}Cs lake sediments)

Among the 13 organic macroremains analysed for ^{14}C, 4 dates were removed from the age model calculation because they were sampled at the base of event deposits and yielded ages older than the general trend (Fig. S4): Poz-121305; Poz-121306; Poz-120585 and Poz-133271 (see position in Fig. S2). The Poz-133277 and Poz-144680 dates, which were the shallowest samples of the core, were also removed from the age model as they provided the oldest calibrated ages among the dated samples. Finally, only 4 dates were kept for age-depth modelling, because Poz120584, Poz133273, and Poz121164 were also too old to fit the general

trend of ^{14}C ages and probably correspond to reworked materials (Table 2). The core depths of the Poz-144609, Poz-133272, Poz-133275 and Poz-133276 dates were computed on the master core depth (216 cm) using the correlation between cores (Fig. S2).

Table 2 should be inserted here (^{14}C dates)

To produce an age-depth model with radionuclides and radiocarbon ages, a smooth spline model (smoothing = 0.45, Fig. 6) was used in the clam package on event-free master core depth (155 cm; Sabatier et al., 2022). According to the age-depth model (Fig. 6), the bottom of the PLG-03 core is dated at 1581 yr cal CE at 106.8 cm (2σ: 1514-1640). The uncertainties (2σ) of the age-depth model do not allow to properly constraint the time period of the Pb peaks (between 56.5 and 82.5 cm, Fig. 2). To improve the model accuracy around the period of interest (Fig. 6, dashed gray line), an additional historical date was implemented in the general model, which corresponds to the beginning of smelting at the Peisey-Nancroix mining site (1745 ± 1 yr cal CE, at 82 cm). These changes are visible in purple in Fig. 6 to produce a second model (in blue). According to the age-depth model, the sediment accumulation rate (SR) was relatively constant between 0 and 100 cm varying from 1.15 to 1.45 $mm.y^{-1}$. Then, it increases in depth until 150 cm to reach 2.08 $mm.y^{-1}$.

Figure 6 should be inserted here

5.6. Anthropogenic Pb inventories

5.6.1 Lake sediment anthropogenic Pb inventories

The accumulation rate of anthropogenic Pb (AR_{Pb_ANTH}) calculated on nine selected samples yielded similar results with the two methods used (elemental and isotopic; equations (2) et (3)), (Fig. 7B). In order to provide the highest resolution, the element-based *AR*s have been preferred. From 1593 to 1713 yr cal CE, the AR_{Pb_ANTH} is non-significant. The oldest significant rise in

447 AR_{Pb_ANTH} is dated to 1731 CE ± 10 yr. It then peaked between 1750 and 1790, i.e. during the
448 oldest smelting period known in Peisey-Nancroix (Fig. 7C). The most recent samples present
449 an AR_{Pb_ANTH} very close to pre-industrial values, even though several peaks in ARs are observed
450 along the decreasing trend that followed the closure of the Peisey-Nancroix metallurgical site
451 in 1824.

452 The two peaks of contamination evidenced both by the core scanner XRF data and computed
453 ARs seem to mirror the ore production data from the local smelting site. It is characterised by
454 two phases of activity separated by an industrial pause between 1792 and 1804 (Fig. 7C).
455 However, the age-depth model presents large uncertainties and such an interpretation must be
456 discussed cautiously.
457 In order to mitigate the effect of the age-model uncertainties, contaminating Pb inventories were
458 computed over large time periods using equation (5): prior the smelting period ($Inv._{\text{Pb prior-smelting}}$
459 1593-1745 yr cal CE; i.e. 152 years), during the smelting period ($Inv._{\text{Pb smelting}}$ 1745-1824 yr cal
460 CE; i.e. 79 years), after the smelting period ($Inv._{\text{Pb post-smelting}}$; 1824-2019 yr cal CE; i.e. 195
461 years), as well as the total inventory (from 1593 to 2019 yr cal CE; i.e. 426 years). A total of
462 19.3 $g.m^{-2}$ of Pb due to anthropogenic activities has been cumulated in PLG-03 core from 1593
463 to 2019 yr cal CE; with less than 0.1% accumulated prior to the period of local smelting activity.
464 During the 79 years of the smelting period ($Inv._{\text{Pb smelting}}$) a total of 7.8 $g.m^{-2}$ of Pb has been
465 accumulated at the bottom of the lake, which represents a mean accumulation rate of ca. 98
466 $mg.m^{-2}.y^{-1}$. Such inventory is comparable to that of the post-smelting period (10.7 $g.m^{-2}$),
467 although the mean accumulation rate was slightly lower during this latest period (ca. 55 $mg.m^{-2}.y^{-1}$). These inventories account for 40% and 54% of the total inventory of the core,
469 respectively.

470 *5.6.2 Soil anthropogenic Pb inventories*

The anthropogenic Pb (Pb_{ANTH}) was determined in soils using the elemental method. Thorium was used as the immobile element, as the Pb/Th ratios remained constant in the deepest soil horizons whatever their lithology. The anthropogenic contribution of Pb in soils ranges from 54% to 89% of the total Pb (Fig 4). The highest percentages were found in the vicinity of the lake (A1; 86%) or within relatively flat areas higher in the catchment area (A2; 89% and B6; 86%), i.e. in zones of potential accumulation. The lowest percentages were observed in A3 (54%), A4 (65%), and B3 (70%), which are located in steep areas, and are thus more exposed to erosion. The inventories of anthropogenic Pb calculated from equation -6) for each superficial soil sample (20-cm thick) vary from 1.6 to 9.0 $g.m^{-2}$ (4.9 ± 2.5, Table 3).

6. Discussion

6.1 Recording of local ore smelting activities

Lake La Plagne sediments have recorded Pb enrichments (up to EF = 5) during the smelting period in Peisey-Nancroix (Fig. 2), between 1745 and 1824. The Pb isotopic signature of these enriched sediments is close to that of the local ore (Fig. 4). As Pb isotopes do not fractionate during ore smelting (Baron et al., 2006; Cui and Wu, 2011; Shiel et al., 2010), the observed Pb enrichment likely results from the deposition of atmospheric fallouts emitted during smelting of the Peisey-Nancroix Pb-rich ore, 7 km upwind. Such a recording of local mining activity in lake sediments is consistent with the literature (Carvalho and Schulte, 2020; Elbaz-Poulichet et al., 2020).

6.2 Local vs regional anthropogenic Pb accumulation rates

In addition to the local anthropogenic signal, lake sediments may record more regional or even global anthropogenic activities (Brännvall et al., 2001, 1999; Mariet et al., 2018). In order to investigate the importance of the regional signal, the anthropogenic Pb inventories of Lake La Plagne were compared with the anthropogenic Pb inventories of Lake Anterne, which only

recorded the regional signal (no local mining nor smelting activity). Lake Anterne is located 56 km as the crow flies from Lake La Plagne (Massif des Aiguilles Rouges, Fig. 1B). Arnaud et al. (2004) estimated anthropogenic Pb fluxes since 1725 CE in Lake Anterne sediments, showing no significant Pb contamination prior the end of the 19th century.

The focus factor (equation 7) estimated from the $^{210}Pb_{ex}$ inventories of Lake La Plagne and Lake Anterne allows calculating a surplus of 7.3 g.m^{-2} of anthropogenic Pb (equation 8) for Lake La Plagne (Table 3). Lake La Plagne is therefore enriched 30 times compared to the regional signal recorded in Lake Anterne during smelting in Peisey-Nancroix (1745-1824). Such an enrichment confirms that the anthropogenic Pb recorded in Lake La Plagne results from atmospheric fallouts during smelting rather than from a more regional signal.

Table 3 should be inserted here (Inventories for soil and lake)

Indeed, during the period of maximum ore production in Peisey-Nancroix, the anthropogenic Pb accumulation rate (i.e., anthropogenic flux, AR_{Pb_ANTH}) reached 183 ± 67 mg.m^{-2}.y^{-1}. During that period, the variations in anthropogenic Pb fluxes are consistent with the evolution of the ore production, from an average AR_{Pb_ANTH} of 113 mg.m^{-2}.y^{-1} between 1745 and 1792 yr cal CE (n = 7) to an AR_{Pb_ANTH} of 74 mg.m^{-2}.y^{-1} between 1804-1824 yr cal CE (n = 5, Fig. 7).

Anthropogenic Pb fluxes recorded at Lake La Plagne during smelting activities are high. No such high AR_{Pb_ANTH} were recorded during the Roman, Medieval or recent times in the western Alps (Elbaz-Poulichet et al., 2020; Guédron et al., 2016; Simonneau et al., 2014; Giguet-Covex et al., 2011; Thevenon et al., 2011a, 2011b; Guyard et al., 2007; Arnaud et al., 2004). Similar AR_{Pb_ANTH} (~ 120 mg.m^{-2}.y^{-1}) was only recorded in a peat bog from Příbram in Czech Republic, in relation with the production of 5000 t of Pb from Pb-ore in the 19th and 20th centuries (Mihaljevič et al., 2006).

The total amount of anthropogenic Pb accumulated in the Lake La Plagne sediment core ($Inv._{Pb\_anth}$) corresponds to a total of 19.3 g.m^{-2}, exceeding the Pb inventories estimated from

various archives sampled near Pb-Ag mining districts (Bacardit et al., 2012; Yang and Rose, 2005). For example, the Etang de la Gruère (Switzerland, Shotyk et al., 1998) or the Etang Mort (Spain, Hansson et al., 2017) accumulated less than 9 $g.m^{-2}$ of anthropogenic Pb during Roman and Medieval times in peat bogs. The local industrial contamination may hence contribute to a much higher Pb load in the environment than both the global Roman and medieval contaminations.

Remote mountain areas have the potential to store global, regional, and local contaminations. Mountain soils have an isotopic signature ranging between anthropogenic sources driven by industrial emissions and the uncontaminated background (Lahd Geagea et al., 2008; Hernandez et al., 2003). Present-day remobilisation of past deposited leaded gasoline has also been identified as a lake contaminant (Hansson et al., 2017; Bacardit and Camarero, 2010). In this study, the Pb isotopic compositions of lake sediments and catchment soils do not show any contribution from leaded gasoline or any anthropogenic sources of Pb other than local metallurgy (Fig 4C). In lake sediments, a small Pb peak similar to the one recorded in Lake Anterne was identified in Lake La Plagne between 1965 and 1975 yr cal CE, but no Pb isotope data can confirm the presence of gasoline Pb. Lake Redò (Central Pyrenees, Spain), which is located between two mining districts (~20 km apart) operated during the last century, has evidenced no trace of gasoline Pb. However, in areas previously contaminated by smelting of nearby Pb-ore mines, the signal of Pb contamination may have been weakened due to the dilution caused by the presence of inherited Pb for several hundred years. The same seems to have occurred in Lake La Plagne. Very distant mountain catchment areas may thus have been preserved from regional Pb fluxes, showing no or minor contribution (Lake La Plagne, this study; Lake Redò, Camarero et al. 1998) in contrast to lakes located closer to urban centres (Lake Anterne, Arnaud et al. 2004, Giguet-Covex et al. 2011; Lake Lucerne, Thevenon et al. 2011, Elbaz-Poulichez et al., 2020).

6.3 Long persistence of anthropogenic Pb in lake sediments

Unlike other archives, such as ombrotrophic peats that record direct atmospheric deposition, the accumulation of anthropogenic contaminants in sediments is the sum of the atmospheric deposition over the lake itself and a fraction of the deposition over the entire catchment area that has been remobilised by erosion (Bacardit and Camarero, 2010; Rose et al., 2012). Consequently, the larger the catchment and the more connected it is to the lake, the higher the contaminant inventory will be for a similar atmospheric flux.

During the post-smelting period, $Inv_{.Pb}$ of Lake La Plagne is 5 times higher than the $Inv._{Pb}$ in Lake Anterne (10.5 and 2.2 $g.m^{-2}$, respectively, Table 3). A $Surplus_{Pb}$ of 5.9 $g.m^{-2}$ is hence recorded in Lake La Plagne (+56 % compared to the regional signal) during the post-smelting period (1824-1999 yr cal CE). However, the difference in AR_{Pb_ANTH} between Lake La Plagne and Lake Anterne tends to decrease (Fig. 8A) over the most recent period (1970-1999 yr cal CE), with a local $Surplus_{Pb}$ of 0.8 $g.m^{-2}$. These Pb inventories hence indicate a significant anthropogenic Pb surplus in Lake La Plagne since the smelter has shut down (Fig 8B). As no other source of anthropogenic Pb was identified apart from metallurgic emissions, these results suggest the presence of a pervasive source of metallurgic Pb in the catchment area due to the remobilisation of lead fallouts that had accumulated in soils during the 79 years of metallurgical activities.

Anthropogenic Pb remobilisation is confirmed by the Pb isotopic compositions of the shallowest sediments, which show a mixing between the local isotopic background and the local ore, with a remaining contribution of the anthropogenic Pb of 20 to 25% of the total Pb. Hence, a small proportion of the Pb emitted during smelting is still being eroded from the catchment soils nowadays and transferred to the lake. Therefore, soils within Lake La Plagne catchment area could be considered as a long-term, slowly emptying, source of anthropogenic Pb contamination. Such a process has been suggested by other studies (Yang et al., 2002, 2001).

6.4 Long-lasting remobilisation of legacy Pb from soil

A decreasing trend in anthropogenic Pb fluxes from local inherited smelting contamination was evidenced in the sediments of Lake La Plagne, which now tends to be negligible (~20 $mg.m^{-2}.y^{-1}$, Fig 8A). This suggests that less and less anthropogenic Pb has been washed out from the catchment over time (Fig 8B). However, superficial soils from the catchment are not yet free of local anthropogenic Pb (Fig. 4). These combined observations suggest that the most mobile Pb has already been washed out into the lake, and that the remaining Pb might be relatively stable. Further investigations on the lead speciation should be led to confirm this hypothesis. The current inventories of anthropogenic Pb in soils seems greatly influenced by the catchment topography (Fig. 4). Indeed, the most contaminated soils are located at the footstep of the catchment area and/or on the flattest areas, where the matter eroded upstream can accumulate. In contrast, soil samples collected uphill and/or on the steepest slopes present the lowest Pb-inventories because of more intense erosion. These observations confirm the hypothesis of a progressive washing out of past lead fallouts since the end of metallurgical activities, through physical erosion processes.

7. Conclusion

This study highlights the importance of a multi-compartment approach to investigate the long-term persistence and remobilisation of anthropogenic contaminants in the critical zone. In the Lake La Plagne catchment (northern French Alps), Pb isotopes have demonstrated that Pb emitted during smelting in Peisey-Nancroix (1745-1824) fell out on the lake surface and the surrounding soils. The lake sediments have recorded this primary anthropogenic contamination, reaching 180 $mg.m^{-2}.y^{-1}$ of Pb during the maximum production of Pb. Pb isotope ratios and estimated fluxes of anthropogenic Pb in more recent sediments provide evidence of anthropogenic Pb transfer from the catchment to the lake for the last 200 years. If such a transfer decreases over time, the catchment soils still contain a significant stock of anthropogenic Pb

(54-89%) that is considered as a secondary source of anthropogenic Pb dispersal into the environment. The spatial distribution of anthropogenic Pb in the catchment soils is closely linked to the topographical changes: (i) anthropogenic Pb is depleted upslope whereas it is stocked downslope by the lake, and (ii) anthropogenic Pb is accumulated on flat surfaces but is eroded in steeper slopes. Therefore, smelting that occurred 200 years ago has contributed to increasing the stock of anthropogenic Pb in both soils and lake sediments in the long-term (several centuries). Such a diffuse contamination due to atmospheric fallouts during smelting activity, the long-term persistence and remobilisation of the anthropogenic contaminants, should better be considered when investigating the mining legacy and mitigation strategies.

8. Acknowledgement

This work was supported by the French National Program EC2CO (Ecosphère Continentale et Côtière) and by the MITI Program (Mission pour les initiatives transverses et interdisciplinaire) of the CNRS. The authors acknowledge the work of L. Marchal (EDYTEM) regarding field work and soil density measurements. The authors are thankful to the two anonymous reviewers and the editor for their constructive remarks that helped improving the manuscript.

9. Appendix A – Supplementary material

Supplementary material is available at the following link

10. References

Appleby, P.G., Richardson, N., Nolan, P.J., 1991. 241Am dating of lake sediments. Hydrobiologia 214, 35–42. https://doi.org/10.1007/BF00050929

Arnaud, F., Lignier, V., Revel, M., Desmet, M., Beck, C., Pourchet, M., Charlet, F., Trentesaux, A., Tribovillard, N., 2002. Flood and earthquake disturbance of 210Pb geochronology (Lake Anterne, NW Alps). Terra Nova 14, 225–232. https://doi.org/10.1046/j.1365-3121.2002.00413.x

Arnaud, F., Revel-Rolland, M., Bosch, D., Winiarski, T., Desmet, M., Tribovillard, N., Givelet, N., 2004. A 300 year history of lead contamination in northern French Alps reconstructed from distant lake sediment records. J. Environ. Monit. 6, 448–456. https://doi.org/10.1039/B314947A

Bacardit, M., Camarero, L., 2010. Modelling Pb, Zn and As transfer from terrestrial to aquatic ecosystems during the ice-free season in three Pyrenean catchments. Sci. Total

Environ., Special Section: Integrating Water and Agricultural Management Under Climate Change 408, 5854–5861. https://doi.org/10.1016/j.scitotenv.2010.07.088
Bacardit, M., Krachler, M., Camarero, L., 2012. Whole-catchment inventories of trace metals in soils and sediments in mountain lake catchments in the Central Pyrenees: Apportioning the anthropogenic and natural contributions. Geochim. Cosmochim. Acta, Environmental Records of Anthropogenic Impacts 82, 52–67. https://doi.org/10.1016/j.gca.2010.10.030
Barbier, V. (1828-1898) A. du texte, 1875. La Savoie industrielle. Mines et métaux. Chaux, ciments, plâtres, poteries et tuileries. Horlogerie. Industries diverses / par V. Barbier,...
Baron, S., Carignan, J., Laurent, S., Ploquin, A., 2006. Medieval lead making on Mont-Lozère Massif (Cévennes-France): Tracing ore sources using Pb isotopes. Appl. Geochem. 21, 241–252. https://doi.org/10.1016/j.apgeochem.2005.09.005
Blaauw, M., 2010. Methods and code for 'classical' age-modelling of radiocarbon sequences. Quat. Geochronol. 5, 512–518. https://doi.org/10.1016/j.quageo.2010.01.002
Brännvall, M.-L., Bindler, R., Emteryd, O., Nilsson, M., Renberg, I., 1997. Stable Isotope and Concentration Records of Atmospheric Lead Pollution in Peat and Lake Sediments in Sweden. Water. Air. Soil Pollut. 100, 243–252. https://doi.org/10.1023/A:1018360106350
Brännvall, M.-L., Bindler, R., Emteryd, O., Renberg, I., 2001. Four thousand years of atmospheric lead pollution in northern Europe: a summary from Swedish lake sediments. J. Paleolimnol. 25, 421–435. https://doi.org/10.1023/A:1011186100081
Brännvall, M.-L., Bindler, R., Renberg, I., Emteryd, O., Bartnicki, J., Billström, K., 1999. The Medieval Metal Industry Was the Cradle of Modern Large-Scale Atmospheric Lead Pollution in Northern Europe. Environ. Sci. Technol. 33, 4391–4395. https://doi.org/10.1021/es990279n
Bruel, R., Sabatier, P., 2020. serac: an R package for ShortlivEd RAdionuclide chronology of recent sediment cores. J. Environ. Radioact. 225, 106449. https://doi.org/10.1016/j.jenvrad.2020.106449
Camizuli, E., Monna, F., Bermond, A., Manouchehri, N., Besançon, S., Losno, R., van Oort, F., Labanowski, J., Perreira, A., Chateau, C., Alibert, P., 2014. Impact of historical mining assessed in soils by kinetic extraction and lead isotopic ratios. Sci. Total Environ. 472, 425–436. https://doi.org/10.1016/j.scitotenv.2013.10.103
Camizuli, E., Scheifler, R., Garnier, S., Monna, F., Losno, R., Gourault, C., Hamm, G., Lachiche, C., Delivet, G., Chateau, C., Alibert, P., 2018. Trace metals from historical mining sites and past metallurgical activity remain bioavailable to wildlife today. Sci. Rep. 8, 3436. https://doi.org/10.1038/s41598-018-20983-0
Carignan, J., Hild, P., Mevelle, G., Morel, J., Yeghicheyan, D., 2001. Routine Analyses of Trace Elements in Geological Samples using Flow Injection and Low Pressure On-Line Liquid Chromatography Coupled to ICP-MS: A Study of Geochemical Reference Materials BR, DR-N, UB-N, AN-G and GH. Geostand. Geoanalytical Res. 25, 187–198. https://doi.org/10.1111/j.1751-908X.2001.tb00595.x
Carvalho, F., Schulte, L., 2020. Reconstruction of mining activities in the Western Alps during the past 2500years from natural archives. Sci. Total Environ. 750, 141208. https://doi.org/10.1016/j.scitotenv.2020.141208
Cloquet, C., Carignan, J., Libourel, G., Sterckeman, T., Perdrix, E., 2006. Tracing Source Pollution in Soils Using Cadmium and Lead Isotopes. Environ. Sci. Technol. 40, 2525–2530. https://doi.org/10.1021/es052232+
Corella, J.P., Sierra, M.J., Garralón, A., Millán, R., Rodríguez-Alonso, J., Mata, M.P., de Vera, A.V., Moreno, A., González-Sampériz, P., Duval, B., Amouroux, D., Vivez, P., Cuevas, C.A., Adame, J.A., Wilhelm, B., Saiz-Lopez, A., Valero-Garcés, B.L., 2021.

675 Recent and historical pollution legacy in high altitude Lake Marboré (Central
676 Pyrenees): A record of mining and smelting since pre-Roman times in the Iberian
677 Peninsula. Sci. Total Environ. 751, 141557.
678 https://doi.org/10.1016/j.scitotenv.2020.141557
679 Cui, J., Wu, X., 2011. AN EXPERIMENTAL INVESTIGATION ON LEAD ISOTOPIC
680 FRACTIONATION DURING METALLURGICAL PROCESSES: Lead isotopic
681 fractionation during metallurgical processes. Archaeometry 53, 205–214.
682 https://doi.org/10.1111/j.1475-4754.2010.00548.x
683 De Vleeschouwer, F., Gérard, L., Goormaghtigh, C., Mattielli, N., Le Roux, G., Fagel, N.,
684 2007. Atmospheric lead and heavy metal pollution records from a Belgian peat bog
685 spanning the last two millenia: Human impact on a regional to global scale. Sci. Total
686 Environ. 377, 282–295. https://doi.org/10.1016/j.scitotenv.2007.02.017
687 Deloule, E., Allegre, C.J., Doe, B.R., 1986. Lead and sulfur isotope microstratigraphy in
688 galena crystals from mississippi valley-type deposits. Econ. Geol. 81, 1307–1321.
689 https://doi.org/10.2113/gsecongeo.81.6.1307
690 Doucet, F.J., Carignan, J., 2001. Atmospheric Pb isotopic composition and trace metal
691 concentration as revealed by epiphytic lichens:: an investigation related to two
692 altitudinal sections in Eastern France. Atmos. Environ. 35, 3681–3690.
693 https://doi.org/10.1016/S1352-2310(00)00510-0
694 Elbaz-Poulichet, F., Guédron, S., Anne-Lise, D., Freydier, R., Perrot, V., Rossi, M., Piot, C.,
695 Delpoux, S., Sabatier, P., 2020. A 10,000-year record of trace metal and metalloid
696 (Cu, Hg, Sb, Pb) deposition in a western Alpine lake (Lake Robert, France):
697 Deciphering local and regional mining contamination. Quat. Sci. Rev. 228, 106076.
698 https://doi.org/10.1016/j.quascirev.2019.106076
699 Gabrieli, J., Barbante, C., 2014. The Alps in the age of the Anthropocene: the impact of
700 human activities on the cryosphere recorded in the Colle Gnifetti glacier. Rendiconti
701 Lincei 25, 71–83. https://doi.org/10.1007/s12210-014-0292-2
702 Giguet-Covex, C., Arnaud, F., Poulenard, J., Disnar, J.-R., Delhon, C., Francus, P., David, F.,
703 Enters, D., Rey, P.-J., Delannoy, J.-J., 2011. Changes in erosion patterns during the
704 Holocene in a currently treeless subalpine catchment inferred from lake sediment
705 geochemistry (Lake Anterne, 2063 m a.s.l., NW French Alps): The role of climate and
706 human activities. The Holocene 21, 651–665.
707 https://doi.org/10.1177/0959683610391320
708 Guédron, S., Amouroux, D., Sabatier, P., Desplanque, C., Develle, A.-L., Barre, J., Feng, C.,
709 Guiter, F., Arnaud, F., Reyss, J.L., Charlet, L., 2016. A hundred year record of
710 industrial and urban development in French Alps combining Hg accumulation rates
711 and isotope composition in sediment archives from Lake Luitel. Chem. Geol. 431, 10–
712 19. https://doi.org/10.1016/j.chemgeo.2016.03.016
713 Guillevic, F., Rossi, M., Develle, A.-L., Spadini, L., Martins, J.M.F., Arnaud, F., Poulenard,
714 J., 2023. Pb dispersion pathways in mountain soils contaminated by ancient mining
715 and smelting activities. Appl. Geochem. 105556.
716 https://doi.org/10.1016/j.apgeochem.2022.105556
717 Guyard, H., Chapron, E., St-Onge, G., Anselmetti, F.S., Arnaud, F., Magand, O., Francus, P.,
718 Mélières, M.-A., 2007. High-altitude varve records of abrupt environmental changes
719 and mining activity over the last 4000 years in the Western French Alps (Lake
720 Bramant, Grandes Rousses Massif). Quat. Sci. Rev. 26, 2644–2660.
721 https://doi.org/10.1016/j.quascirev.2007.07.007
722 Hansson, S.V., Claustres, A., Probst, A., De Vleeschouwer, F., Baron, S., Galop, D., Mazier,
723 F., Le Roux, G., 2017. Atmospheric and terrigenous metal accumulation over 3000

years in a French mountain catchment: Local vs distal influences. Anthropocene 19, 45–54. https://doi.org/10.1016/j.ancene.2017.09.002
Hansson, S.V., Grusson, Y., Chimienti, M., Claustres, A., Jean, S., Le Roux, G., 2019. Legacy Pb pollution in the contemporary environment and its potential bioavailability in three mountain catchments. Sci. Total Environ. 671, 1227–1236. https://doi.org/10.1016/j.scitotenv.2019.03.403
Heiri, O., Lotter, A.F., Lemcke, G., 2001. Loss on ignition as a method for estimating organic and carbonate content in sediments: reproducibility and comparability of results. J. Paleolimnol. 25, 101–110. https://doi.org/10.1023/A:1008119611481
Hernandez, L., Probst, A., Probst, J.L., Ulrich, E., 2003. Heavy metal distribution in some French forest soils: evidence for atmospheric contamination. Sci. Total Environ. 312, 195–219. https://doi.org/10.1016/S0048-9697(03)00223-7
Hong, S., Candelone, J.-P., Patterson, C.C., Boutron, C.F., 1994. Greenland Ice Evidence of Hemispheric Lead Pollution Two Millennia Ago by Greek and Roman Civilizations. Science 265, 1841–1843. https://doi.org/10.1126/science.265.5180.1841
Kříbek, B., Majer, V., Knésl, I., Keder, J., Mapani, B., Kamona, F., Mihaljevič, M., Ettler, V., Penížek, V., Vaněk, A., Sracek, O., 2016. Contamination of soil and grass in the Tsumeb smelter area, Namibia: Modeling of contaminants dispersion and ground geochemical verification. Appl. Geochem., Special issue of Applied Geochemistry on Environmental Impacts of Mining and Smelting 64, 75–91. https://doi.org/10.1016/j.apgeochem.2015.07.006
Lahd Geagea, M., Stille, P., Gauthier-Lafaye, F., Perrone, Th., Aubert, D., 2008. Baseline determination of the atmospheric Pb, Sr and Nd isotopic compositions in the Rhine valley, Vosges mountains (France) and the Central Swiss Alps. Appl. Geochem. 23, 1703–1714. https://doi.org/10.1016/j.apgeochem.2008.02.004
Le Roux, G., Hansson, S.V., Claustres, A., Binet, S., Vleeschouwer, F.D., Gandois, L., Mazier, F., Simonneau, A., Teisserenc, R., Allen, D., Rosset, T., Haver, M., Ros, L.D., Galop, D., Durantez, P., Probst, A., Sánchez-Pérez, J.M., Sauvage, S., Laffaille, P., Jean, S., Schmeller, D.S., Camarero, L., Marquer, L., Lofts, S., 2020. Trace Metal Legacy in Mountain Environments, in: Biogeochemical Cycles. American Geophysical Union (AGU), pp. 191–206. https://doi.org/10.1002/9781119413332.ch9
Lê, S., Josse, J., Husson, F., 2008. FactoMineR: An R Package for Multivariate Analysis. J. Stat. Softw. 25, 1–18. https://doi.org/10.18637/jss.v025.i01
Leblanc, M., Morales, J.A., Borrego, J., Elbaz-Poulichet, F., 2000. 4,500-YEAR-OLD MINING POLLUTION IN SOUTHWESTERN SPAIN: LONG-TERM IMPLICATIONS FOR MODERN MINING POLLUTION. Econ. Geol. 95, 655–662. https://doi.org/10.2113/gsecongeo.95.3.655
Mariet, A.-L., Monna, F., Gimbert, F., Bégeot, C., Cloquet, C., Belle, S., Millet, L., Rius, D., Walter-Simonnet, A.-V., 2018. Tracking past mining activity using trace metals, lead isotopes and compositional data analysis of a sediment core from Longemer Lake, Vosges Mountains, France. J. Paleolimnol. 60, 399–412. https://doi.org/10.1007/s10933-018-0029-9
Mariet, A.-L., Sarret, G., Bégeot, C., Walter-Simonnet, A.-V., Gimbert, F., 2017. Lead Highly Available in Soils Centuries after Metallurgical Activities. J. Environ. Qual. 46, 1236–1242. https://doi.org/10.2134/jeq2016.12.0469
Martínez-Cortizas, A., Pontevedra-Pombal, X., García-Rodeja, E., Nóvoa-Muñoz, J.C., Shotyk, W., 1999. Mercury in a Spanish Peat Bog: Archive of Climate Change and Atmospheric Metal Deposition. Science 284, 939–942. https://doi.org/10.1126/science.284.5416.939

Mihaljevič, M., Zuna, M., Ettler, V., Šebek, O., Strnad, L., Goliáš, V., 2006. Lead fluxes, isotopic and concentration profiles in a peat deposit near a lead smelter (Příbram, Czech Republic). Sci. Total Environ. 372, 334–344. https://doi.org/10.1016/j.scitotenv.2006.09.019

Monna, F., Camizuli, E., Revelli, P., Biville, C., Thomas, C., Losno, R., Scheifler, R., Bruguier, O., Baron, S., Chateau, C., Ploquin, A., Alibert, P., 2011. Wild Brown Trout Affected by Historical Mining in the Cévennes National Park, France. Environ. Sci. Technol. 45, 6823–6830. https://doi.org/10.1021/es200755n

Monna, F., Hamer, K., Lévêque, J., Sauer, M., 2000. Pb isotopes as a reliable marker of early mining and smelting in the Northern Harz province (Lower Saxony, Germany). J. Geochem. Explor. 68, 201–210. https://doi.org/10.1016/S0375-6742(00)00005-4

Nriagu, J.O., Pacyna, J.M., 1988. Quantitative assessment of worldwide contamination of air, water and soils by trace metals. Nature 333, 134–139. https://doi.org/10.1038/333134a0

Pacyna, J.M., Pacyna, E.G., 2001. An assessment of global and regional emissions of trace metals to the atmosphere from anthropogenic sources worldwide. Environ. Rev. 9, 269–298. https://doi.org/10.1139/a01-012

Preunkert, S., McConnell, J.R., Hoffmann, H., Legrand, M., Wilson, A.I., Eckhardt, S., Stohl, A., Chellman, N.J., Arienzo, M.M., Friedrich, R., 2019. Lead and Antimony in Basal Ice From Col du Dome (French Alps) Dated With Radiocarbon: A Record of Pollution During Antiquity. Geophys. Res. Lett. 46, 4953–4961. https://doi.org/10.1029/2019GL082641

R Core Team, 2022. R: A language and environment for statistical computing.

Reimer, P.J., 2020. Composition and consequences of the IntCal20 radiocarbon calibration curve. Quat. Res. 96, 22–27. https://doi.org/10.1017/qua.2020.42

Renberg, I., Persson, M.W., Emteryd, O., 1994. Pre-industrial atmospheric lead contamination detected in Swedish lake sediments. Nature 368, 323–326. https://doi.org/10.1038/368323a0

Reyss, J.-L., Schmidt, S., Legeleux, F., Bonté, P., 1995. Large, low background well-type detectors for measurements of environmental radioactivity. Nucl. Instrum. Methods Phys. Res. Sect. Accel. Spectrometers Detect. Assoc. Equip. 357, 391–397. https://doi.org/10.1016/0168-9002(95)00021-6

Rose, N.L., Yang, H., Turner, S.D., Simpson, G.L., 2012. An assessment of the mechanisms for the transfer of lead and mercury from atmospherically contaminated organic soils to lake sediments with particular reference to Scotland, UK. Geochim. Cosmochim. Acta, Environmental Records of Anthropogenic Impacts 82, 113–135. https://doi.org/10.1016/j.gca.2010.12.026

Rosman, K.J.R., Ly, C., Van de Velde, K., Boutron, C.F., 2000. A two century record of lead isotopes in high altitude Alpine snow and ice. Earth Planet. Sci. Lett. 176, 413–424. https://doi.org/10.1016/S0012-821X(00)00013-3

Sabatier, P., Moernaut, J., Bertrand, S., Van Daele, M., Kremer, K., Chaumillon, E., Arnaud, F., 2022. A Review of Event Deposits in Lake Sediments. Quaternary 5, 34. https://doi.org/10.3390/quat5030034

Sabatier, P., Poulenard, J., Fanget, B., Reyss, J.-L., Develle, A.-L., Wilhelm, B., Ployon, E., Pignol, C., Naffrechoux, E., Dorioz, J.-M., Montuelle, B., Arnaud, F., 2014. Long-term relationships among pesticide applications, mobility, and soil erosion in a vineyard watershed. Proc. Natl. Acad. Sci. 111, 15647–15652. https://doi.org/10.1073/pnas.1411512111

Shiel, A.E., Weis, D., Orians, K.J., 2010. Evaluation of zinc, cadmium and lead isotope fractionation during smelting and refining. Sci. Total Environ. 408, 2357–2368. https://doi.org/10.1016/j.scitotenv.2010.02.016

Shotyk, W., Weiss, D., Appleby, P.G., Cheburkin, A.K., Frei, R., Gloor, M., Kramers, J.D., Reese, S., Knaap, W.O.V.D., 1998. History of Atmospheric Lead Deposition Since 12,370 14C yr BP from a Peat Bog, Jura Mountains, Switzerland. Science 281, 1635–1640. https://doi.org/10.1126/science.281.5383.1635

Simonneau, A., Chapron, E., Garçon, M., Winiarski, T., Graz, Y., Chauvel, C., Debret, M., Motelica-Heino, M., Desmet, M., Di Giovanni, C., 2014. Tracking Holocene glacial and high-altitude alpine environments fluctuations from minerogenic and organic markers in proglacial lake sediments (Lake Blanc Huez, Western French Alps). Quat. Sci. Rev. 89, 27–43. https://doi.org/10.1016/j.quascirev.2014.02.008

Smith, J.N., 2001. Why should we believe 210Pb sediment geochronologies? J. Environ. Radioact. 55, 121–123. https://doi.org/10.1016/S0265-931X(00)00152-1

Thevenon, F., Graham, N.D., Chiaradia, M., Arpagaus, P., Wildi, W., Poté, J., 2011a. Local to regional scale industrial heavy metal pollution recorded in sediments of large freshwater lakes in central Europe (lakes Geneva and Lucerne) over the last centuries. Sci. Total Environ. 412–413, 239–247. https://doi.org/10.1016/j.scitotenv.2011.09.025

Thevenon, F., Guédron, S., Chiaradia, M., Loizeau, J.-L., Poté, J., 2011b. (Pre-) historic changes in natural and anthropogenic heavy metals deposition inferred from two contrasting Swiss Alpine lakes. Quat. Sci. Rev. 30, 224–233. https://doi.org/10.1016/j.quascirev.2010.10.013

Thienpont, J.R., Korosi, J.B., Hargan, K.E., Williams, T., Eickmeyer, D.C., Kimpe, L.E., Palmer, M.J., Smol, J.P., Blais, J.M., 2016. Multi-trophic level response to extreme metal contamination from gold mining in a subarctic lake. Proc. R. Soc. B Biol. Sci. 283, 20161125. https://doi.org/10.1098/rspb.2016.1125

Wiklund, J.A., Kirk, J.L., Muir, D.C.G., Gleason, A., Carrier, J., Yang, F., 2020. Atmospheric trace metal deposition to remote Northwest Ontario, Canada: Anthropogenic fluxes and inventories from 1860 to 2010. Sci. Total Environ. 749, 142276. https://doi.org/10.1016/j.scitotenv.2020.142276

Yang, H., Rose, N., 2005. Trace element pollution records in some UK lake sediments, their history, influence factors and regional differences. Environ. Int. 31, 63–75. https://doi.org/10.1016/j.envint.2004.06.010

Yang, H., Rose, N.L., Battarbee, R.W., Boyle, J.F., 2002. Mercury and Lead Budgets for Lochnagar, a Scottish Mountain Lake and Its Catchment. Environ. Sci. Technol. 36, 1383–1388. https://doi.org/10.1021/es010120m

Yang, H., Rose, N.L., Boyle, J.F., Battarbee, R.W., 2001. Storage and distribution of trace metals and spheroidal carbonaceous particles (SCPs) from atmospheric deposition in the catchment peats of Lochnagar, Scotland. Environ. Pollut. 115, 231–238. https://doi.org/10.1016/S0269-7491(01)00107-5

11. Figures captions

Figure 1: Location maps of the study area. A) Map of France indicating the study area; B) Location of the lakes of La Plagne and Anterne in the northern French Alps; C) Location of the Peisey-Nancroix mining and smelting areas and of Lake La Plagne along the Ponturin catchment; D) Geological map of Lake La Plagne catchment, showing the location of the soil samples.

Figure 2: Dry bulk density (DBD), $LOI_{550°C}$ and $LOI_{950°C}$ (unit wt. %) and major and trace element contents measured by ICP-OES and ICP-MS (diamond, in wt. % or $mg.kg^{-1}$) for discrete samples along the PLG-03 core as well as major and trace element content profiles measured by EDS-XRF with a 1-mm step (continuous line, in counts per second). Transparent grey rectangles represent the Ca-rich events and events identified during logging by a higher particle size at the base and by a different colour.

Figure 3: Distribution map of surface soils around Lake La Plagne indicating EF_{Pb}, the total Pb content (in $mg.kg^{-1}$) and the anthropogenic Pb content (Pb_{ANTH} in $mg.kg^{-1}$). See text for the calculation of Pb_{ANTH}.

Figure 4: Pb isotope ratios of soils (surface and subsurface soils) and lake sediments compared to the local Pb ore. A) $^{208}Pb/^{206}Pb$ versus $^{206}Pb/^{207}Pb$ ratios; B) $^{208}Pb/^{206}Pb$ versus $^{206}Pb/^{207}Pb$ ratios with subsurface soils in comparison with more radiogenic cargneule rocks; C) $^{207}Pb/^{204}Pb$ versus $^{206}Pb/^{204}Pb$ ratios of soil and lake sediment far from leaded gasoline end-members. The deepest lake sediments are considered representative of the local isotopic background (see text). Error bars are not larger than point size for the environmental samples.

Figure 5: Age-depth model on the continuous sedimentation (events removed) based on, from left to right, $^{210}Pb_{ex}$ activity ($mBq.g^{-1}$), ^{137}Cs activity ($mBq.g^{-1}$), ^{241}Am activity ($mBq.g^{-1}$) and the age model calculated from $^{210}Pb_{ex}$ on the real depth. The light grey lines represent the Ca-rich events removed from the age-depth modelling. C: Chernobyl; NWT: Nuclear Weapon Test.

Figure 6: Age-depth model of the master core combining ^{137}Cs and ^{231}Am peaks with ^{14}C dates. A first general model was built with measured data, with the best calibration date (black line) and its confidence interval (2σ; grey). A second model (in blue) was built with an additional date indicating the historical beginning of smelting at the Peisey-Nancroix mining site (1745 ± 1 yr cal CE, at 82 cm).

Figure 7: A) The ratio ln(Pb/Rb) from EDS-XRF data according to time (age CE) divided into 3 periods: pre-smelting, smelting and post-smelting periods with $^{206}Pb/^{207}Pb$ ratios of 9 samples along PLG-03; B) Accumulation rate of anthropogenic Pb (AR_{Pb_ANTH}) calculated using both the elemental ratio (Rb) and Pb isotopes (equations 2 and 3); C) Historical timeline of the ore production from 1745 to 1865 yr cal CE.

Figure 8: Comparison between Lake La Plagne and Lake Anterne. A) Comparison between AR_{Pb_ANTH} of Lake Anterne and of Lake Plagne; B) Local surplus of Pb_{ANTH} per m^2 calculated from AR_{Pb_ANTH} subtracted from the regional signal (2.12 x Lake Anterne); C) Cumulated Pb_{ANTH} through time in both lakes corresponding to the total inventory recorded in lakes at the sampling date.

12. Tables captions

Table 1: Principal soil properties, trace elements and major contents for superficial soils in Lake La Plagne catchment, divided in two subgroup types according to the underlying lithologies.

Table 2: ^{14}C dates collected in Lake La Plagne cores (PLG), with depth reported on a unique master core depth (MCD). Only 4 dates were kept for the age-depth modelling.

Table 3: Inventories of anthropogenic Pb and $^{210}Pb_{ex}$.

Table 1: Principal soil properties, trace elements and major contents for superficial soils in Lake La Plagne catchment, divided in two subgroup types according to the underlying lithologies.

		Soil properties				Potentially toxic trace elements						Majors elements				
Sample_Name	Lithology	**pH**	**TOC**	**$CaCO_3$**	**CEC**	**As**	**Cd**	**Cu**	**Pb**	**Sb**	**Zn**	**SiO_2**	**Al_2O_3**	**Fe_2O_3**	**MgO**	**CaO**
			%	**%**	**$cmol^+.kg^{-1}$**				**$mg.kg^{-1}$**						**wt. %**	
A2	basement rocks	4.8	6	0.05	8	27.9	0.33	15.3	133	2.36	154	53.2	13.4	5.7	2.5	1.3
A4	basement rocks	4.9	8	0.05	7	26.5	0.25	23.9	39.1	1.63	78.6	51.6	12.6	6.4	2.1	0.6
B1	basement rocks	5.1	9	0.05	14	12.2	0.29	14.3	76.3	1.84	134	49.0	11.9	5.4	2.0	1.2
B3	basement rocks	5.8	9	0.05	21	21.7	0.28	17.5	75.1	6.92	101	50.2	11.9	5.6	2.5	0.8
B4	basement rocks	4.5	6	0.20	7	17.5	0.12	17.7	96.2	4.89	107	58.3	12.2	5.9	2.4	0.1
B5	basement rocks	4.7	7	0.05	8	5.74	0.09	12.9	66.1	1.32	39.2	67.6	8.7	1.7	1.0	0.1
B6	till	5.3	7	0.05	14	6.53	0.26	23.3	102	1.29	102	60.0	10.8	5.1	1.4	0.4
A1	carbonates scree	7.3	12	0.05	31	23.8	0.43	41.2	121	3.26	103	40.9	12.5	4.9	3.2	2.5
A3	carbonates scree	6.6	11	0.05	24	37.5	0.71	20.6	51.3	1.96	99.9	44.7	12.9	3.5	4.4	1.2
B2	carbonates scree	7.2	10	0.05	31	42.6	0.39	25.6	103	3.96	151	48.1	11.3	4.6	2.6	1.5
B7	carbonates scree	7.7	6	0.90	23	22.6	0.72	15.1	101	5.58	169	49.9	13.6	6.0	4.1	1.7
B8	carbonates scree	7.5	7	5.00	18	35.6	0.33	21.9	66.9	1.99	112	42.5	10.8	4.4	6.9	7.3
A5	cargneules	5.6	10	0.05	22	16.0	1.38	19.1	116	2.08	176	43.1	12.0	5.4	3.6	0.7

Table 2: ^{14}C dates collected in Lake La Plagne cores (PLG), with depth reported on a unique master core depth (MCD). Only 4 dates were kept for the age-depth modelling.

Sample Name	Core	MCD depth (in cm)	^{14}C Ages	95% (BC/AD)
Poz-144609	PLG-04	96.3	275 ± 30 BP	1509-1795
Poz-133272	PLG-05	147.7	685 ± 30 BP	1271-1387
Poz-133275	PLG-05	178.5	740 ± 60 BP	1177-1392
Poz-133276	PLG-05	211.5	1430 ± 30 BP	585-656

Table 3 : Inventories of anthropogenic Pb and $^{210}Pbex$

	Inv. $_{Pb\_ANTH}$ ($g.m^{-2}$)				Inv. $^{210}Pb_{ex}$
	Smelting	Post-smelting	Recent	Total	$Bq.m^{-2}$
Lake La Plagne sed.	7.8	8.5	1.8	19.3	17280
Lake Anterne sed.	0.3	1.9	0.4	2.5	8170
Surplus (FF = 2.12)	7.3	4.5	0.8	-	
La Plagne soils				4.88 ± 2.5 (1.64-9)	

Graphical abstract

Between the 18th and 19th century

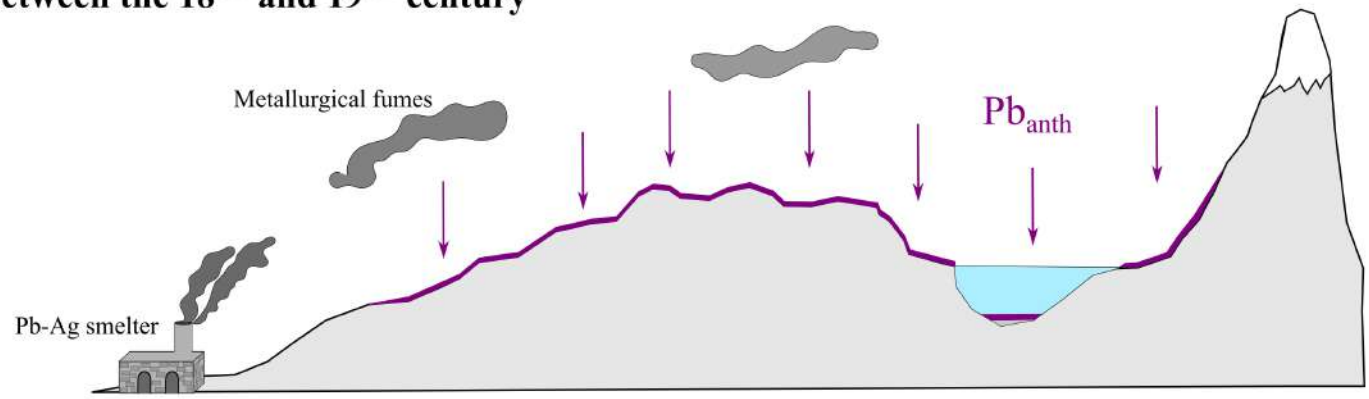

Present-days (200 years after smelter closure)

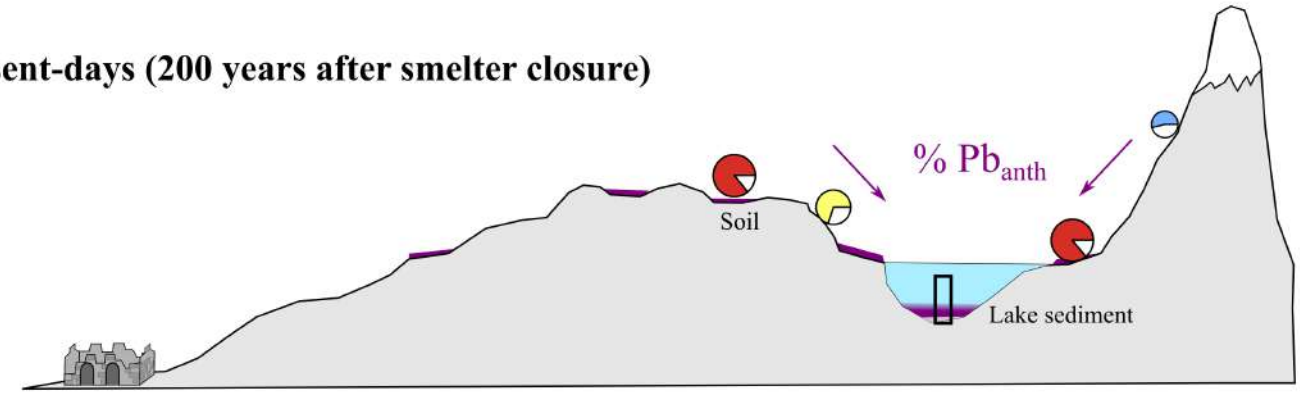

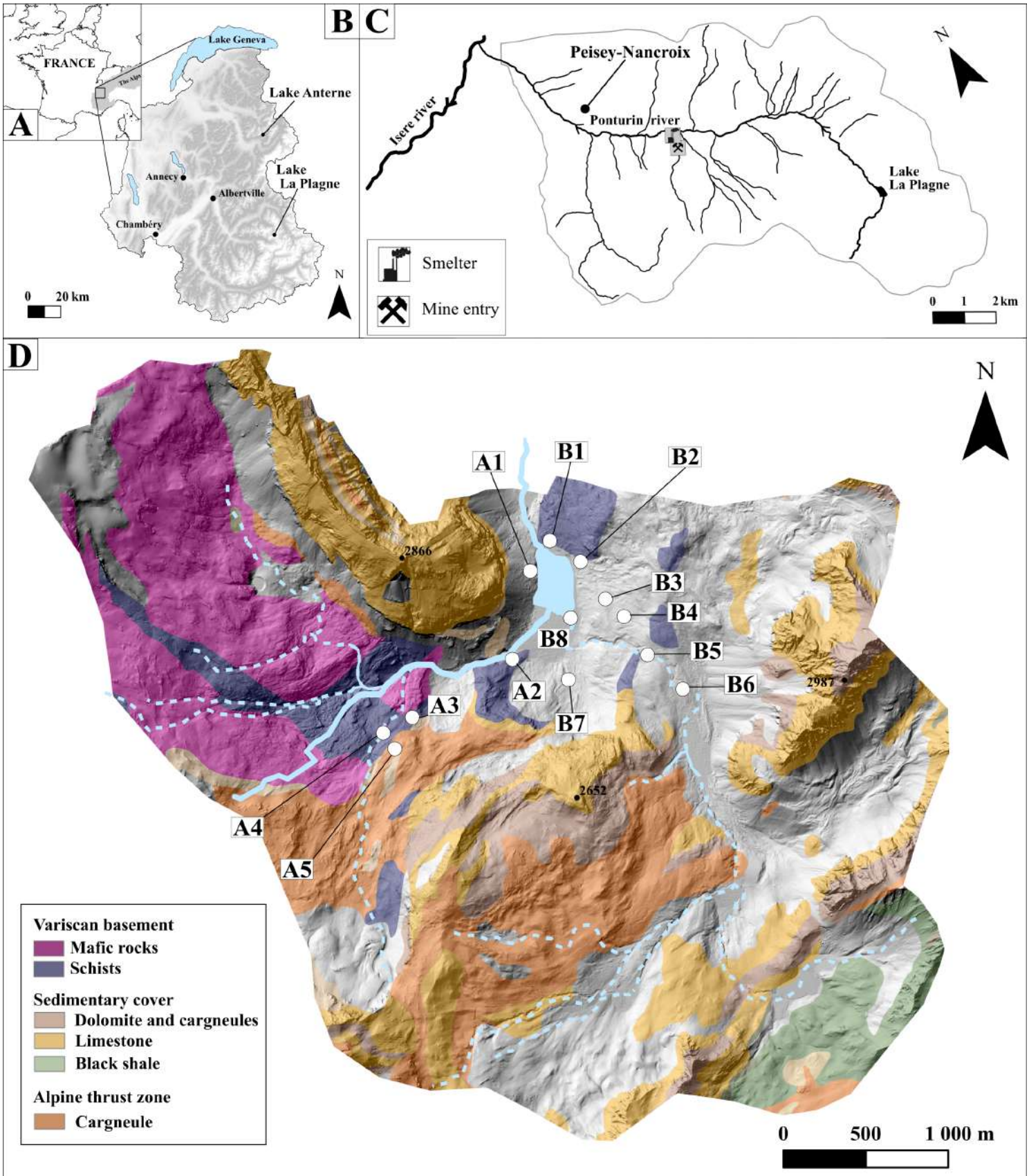

Figure 1: Location maps of the study area. A) Map of France indicating the study area; B) Location of the lakes of La Plagne and Anterne in the northern French Alps; C) Location of the Peisey-Nancroix mining and smelting areas and of Lake La Plagne along the Ponturin catchment; D) Geological map of Lake La Plagne catchment, showing the location of the soil samples.

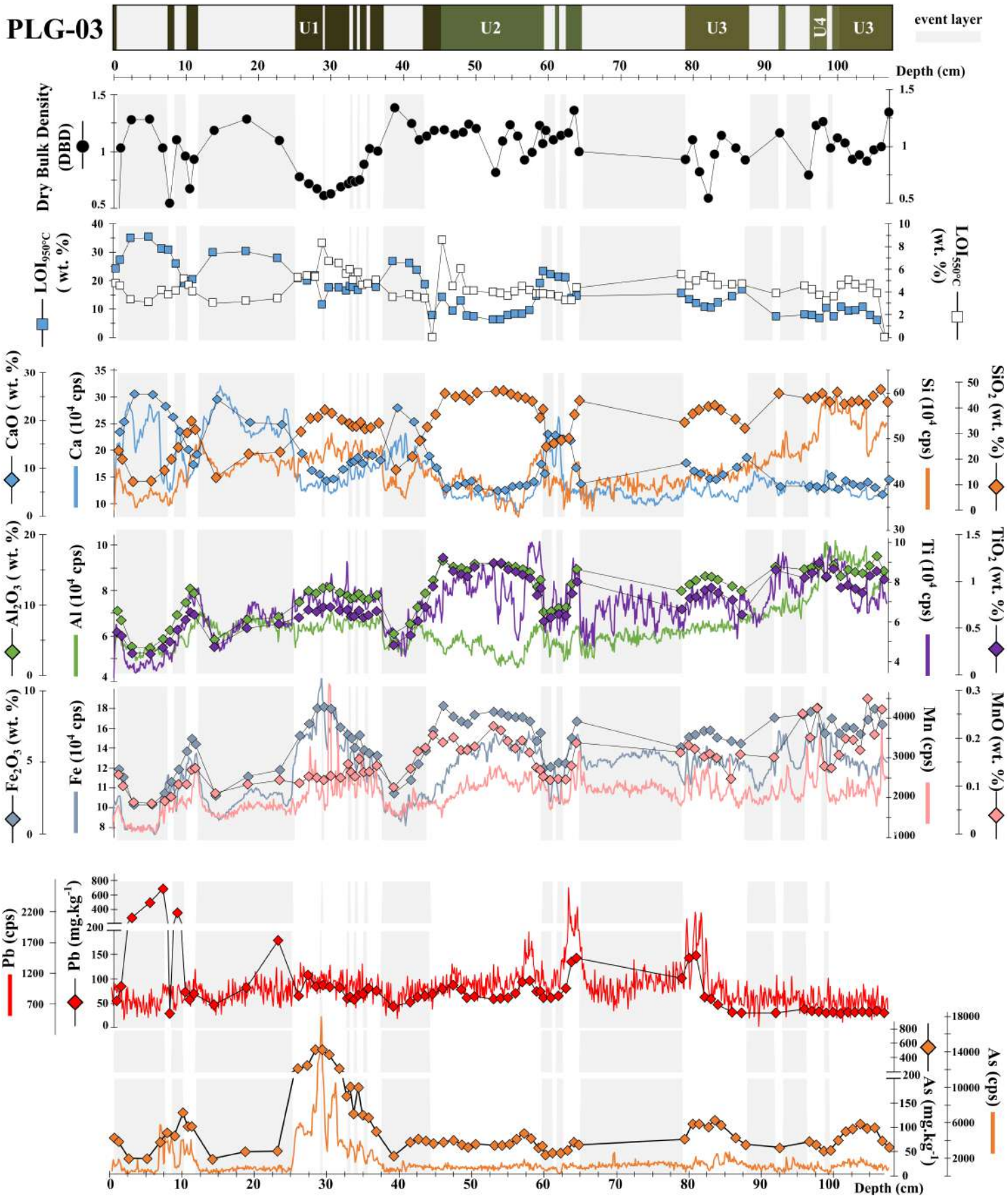

Figure 2: Dry bulk density (DBD), $LOI_{550°C}$ and $LOI_{950°C}$ (unit wt. %) and major and trace element contents measured by ICP-OES and ICP-MS (diamond, in wt. % or $mg.kg^{-1}$) for discrete samples along the PLG-03 core as well as major and trace element content profiles measured by EDS-XRF with a 1-mm step (continuous line, in counts per second). Transparent grey rectangles represent the Ca-rich events and events identified during logging by a higher particle size at the base and by a different colour.

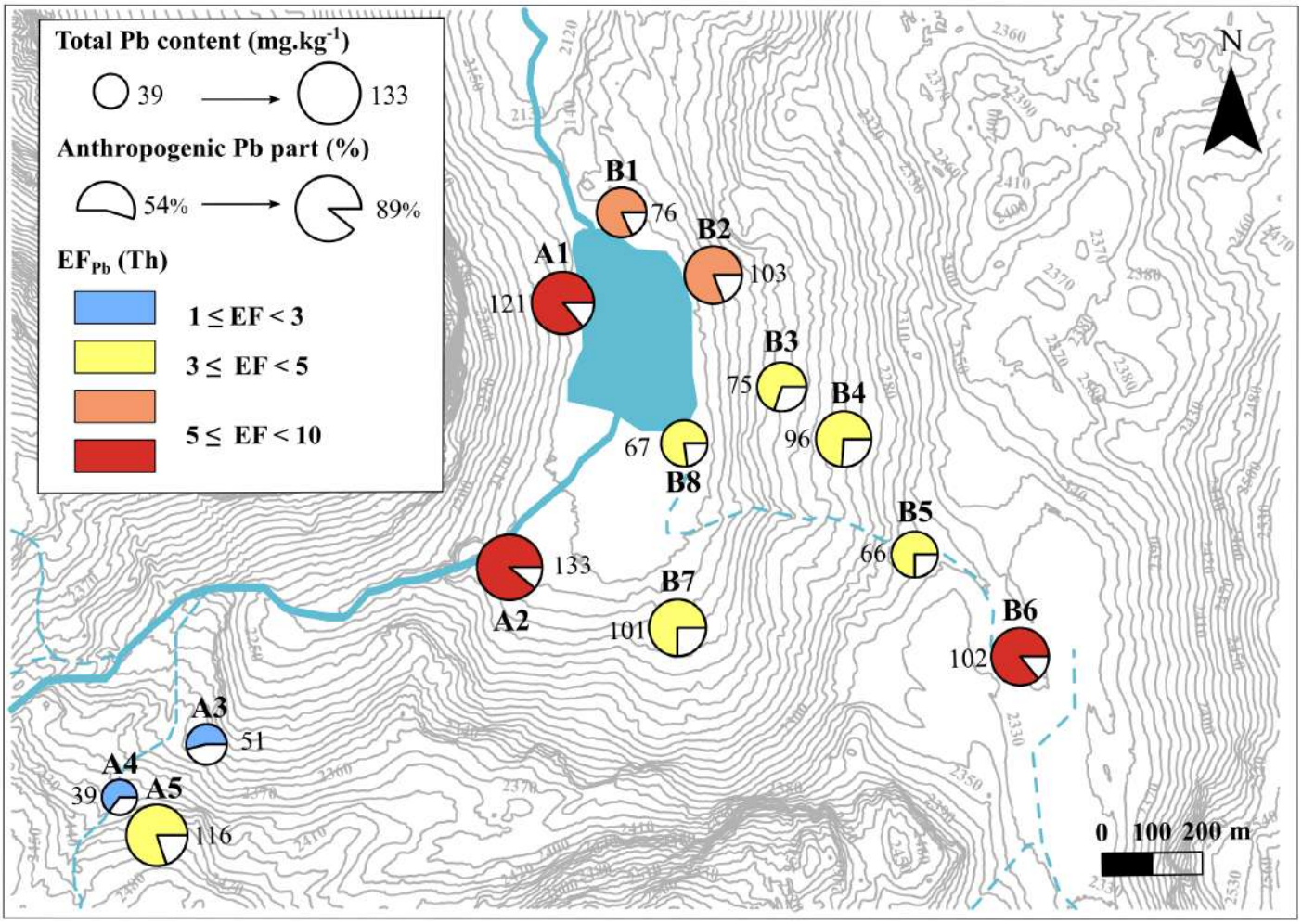

Figure 3: Distribution map of surface soils around Lake La Plagne indicating EF_{Pb}, the total Pb content (in mg.kg^{-1}) and the anthropogenic Pb content (Pb_{ANTH} in mg.kg^{-1}). See text for the calculation of Pb_{ANTH}.

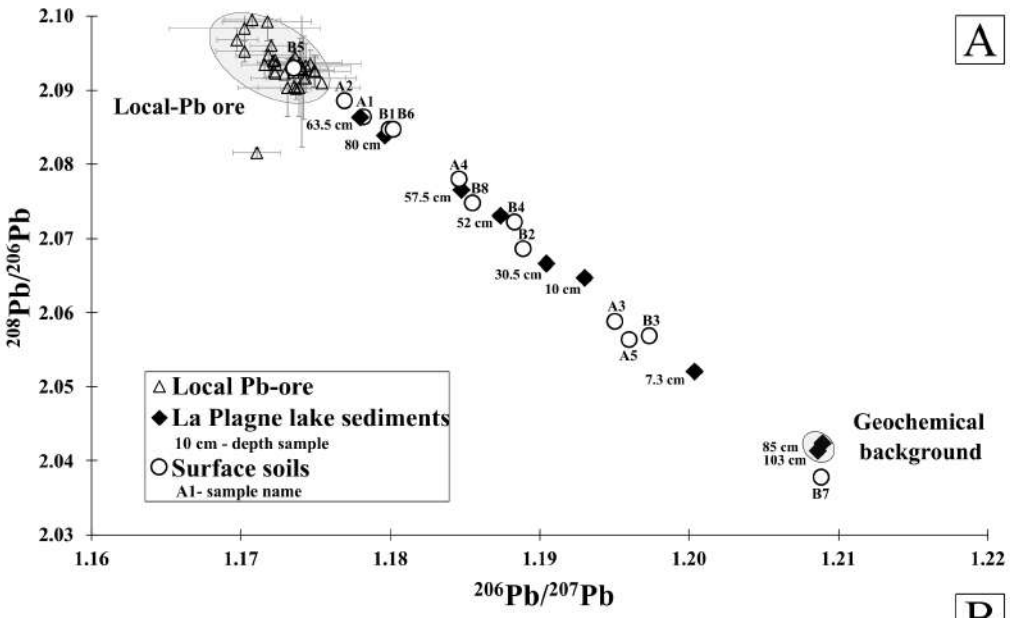

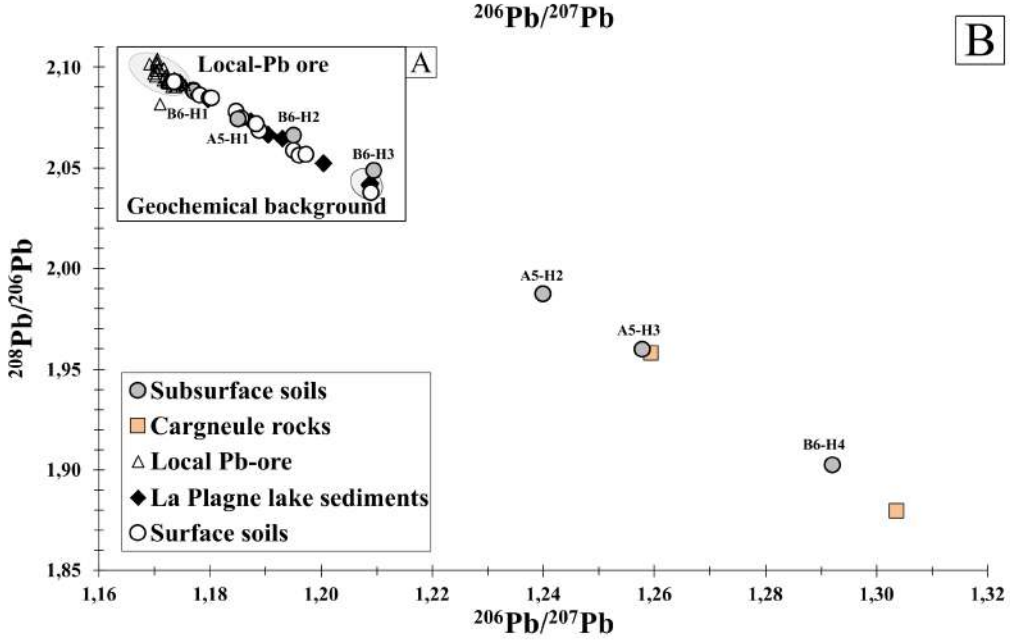

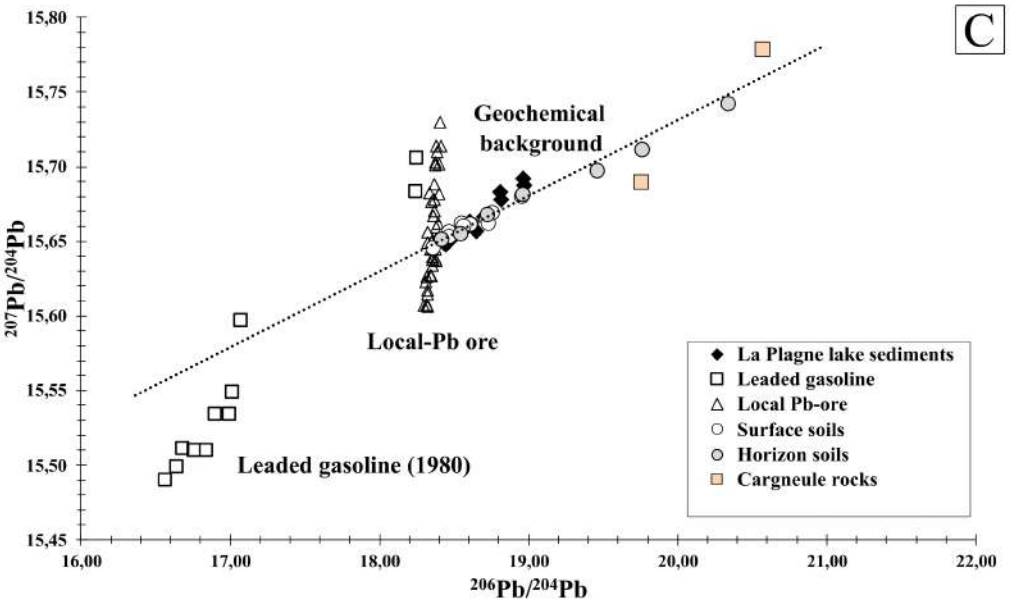

Figure 4: Pb isotope ratios of soils (surface and subsurface soils) and lake sediments compared to the local Pb ore. A) $^{208}Pb/^{206}Pb$ versus $^{206}Pb/^{207}Pb$ ratios; B) $^{208}Pb/^{206}Pb$ versus $^{206}Pb/^{207}Pb$ ratios with subsurface soils in comparison with more radiogenic cargneule rocks; C) $^{207}Pb/^{204}Pb$ versus $^{206}Pb/^{204}Pb$ ratios of soil and lake sediment far from leaded gasoline end-members. The deepest lake sediments are considered representative of the local isotopic background (see text). Error bars are not larger than point size for the environmental samples.

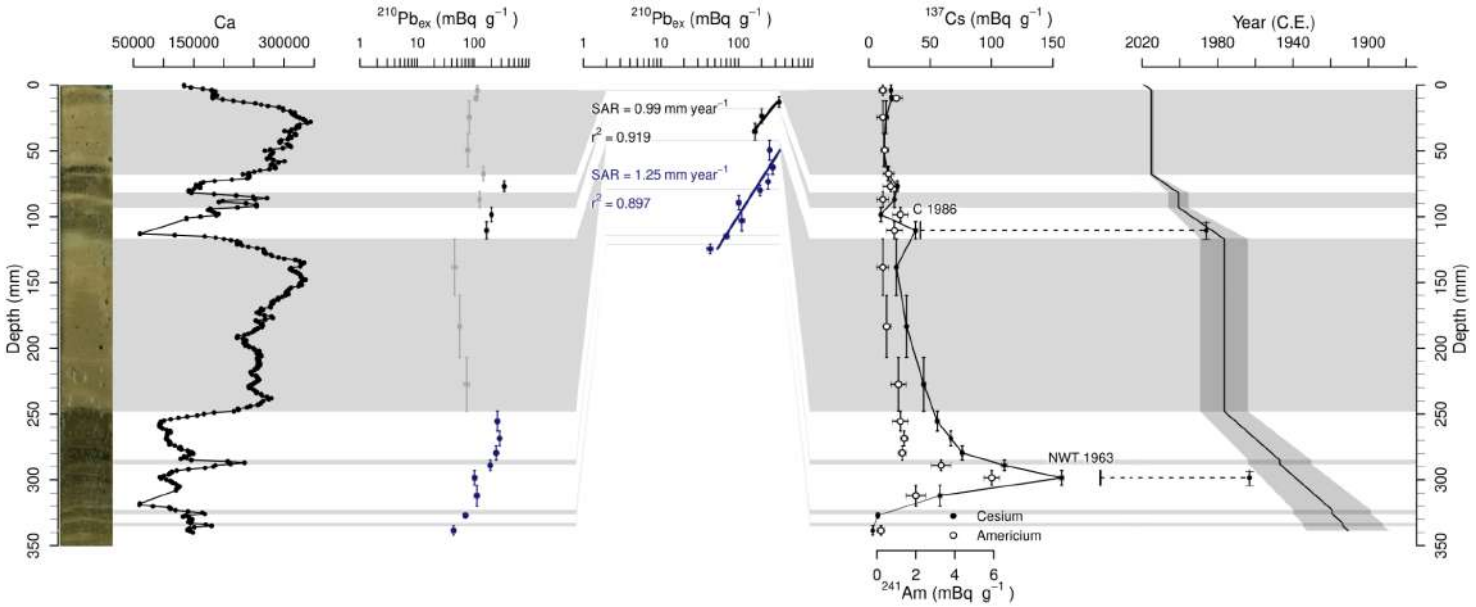

Figure 5: Age-depth model on the continuous sedimentation (event removed) based on, from left to right, $^{210}Pb_{ex}$ activity (mBq.g^{-1}), ^{137}Cs activity (mBq.g^{-1}), ^{241}Am activity (mBq.g^{-1}) and the age model calculated from $^{210}Pb_{ex}$ on the real depth. The light grey lines represent the Ca-rich events removed from the age-depth modelling. C: Chernobyl; NWT: Nuclear Weapon Test.

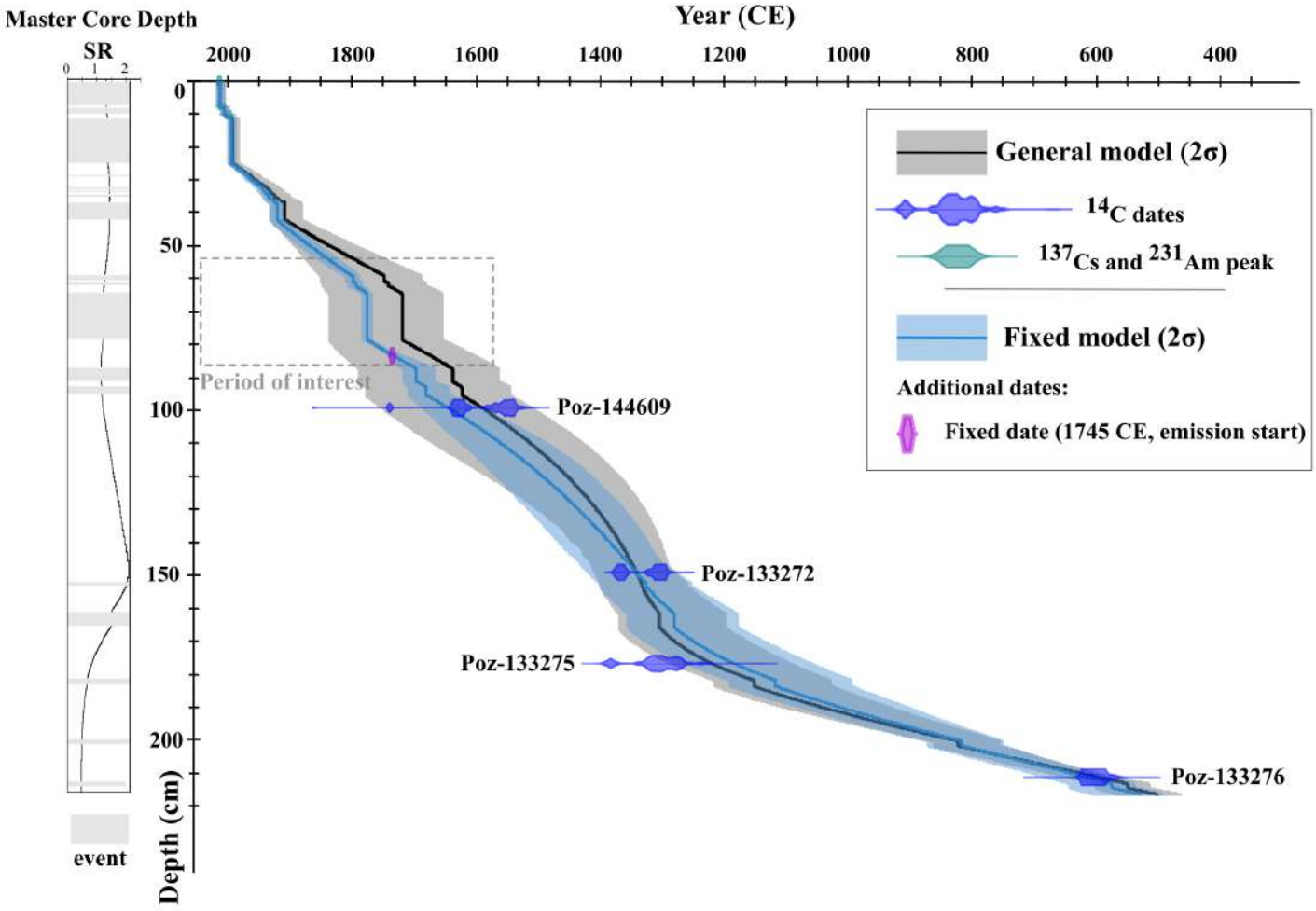

Figure 6: Age-depth model of the master core combining ^{137}Cs and ^{231}Am peaks with ^{14}C dates. A first general model was built with measured data, with the best calibration date (black line) and its confidence interval (2σ, grey). A second model (in blue) was built with an additional date indicating the historical beginning of smelting at the Peisey-Nancroix mining site (1745 ± 1 yr cal CE, at 82 cm).

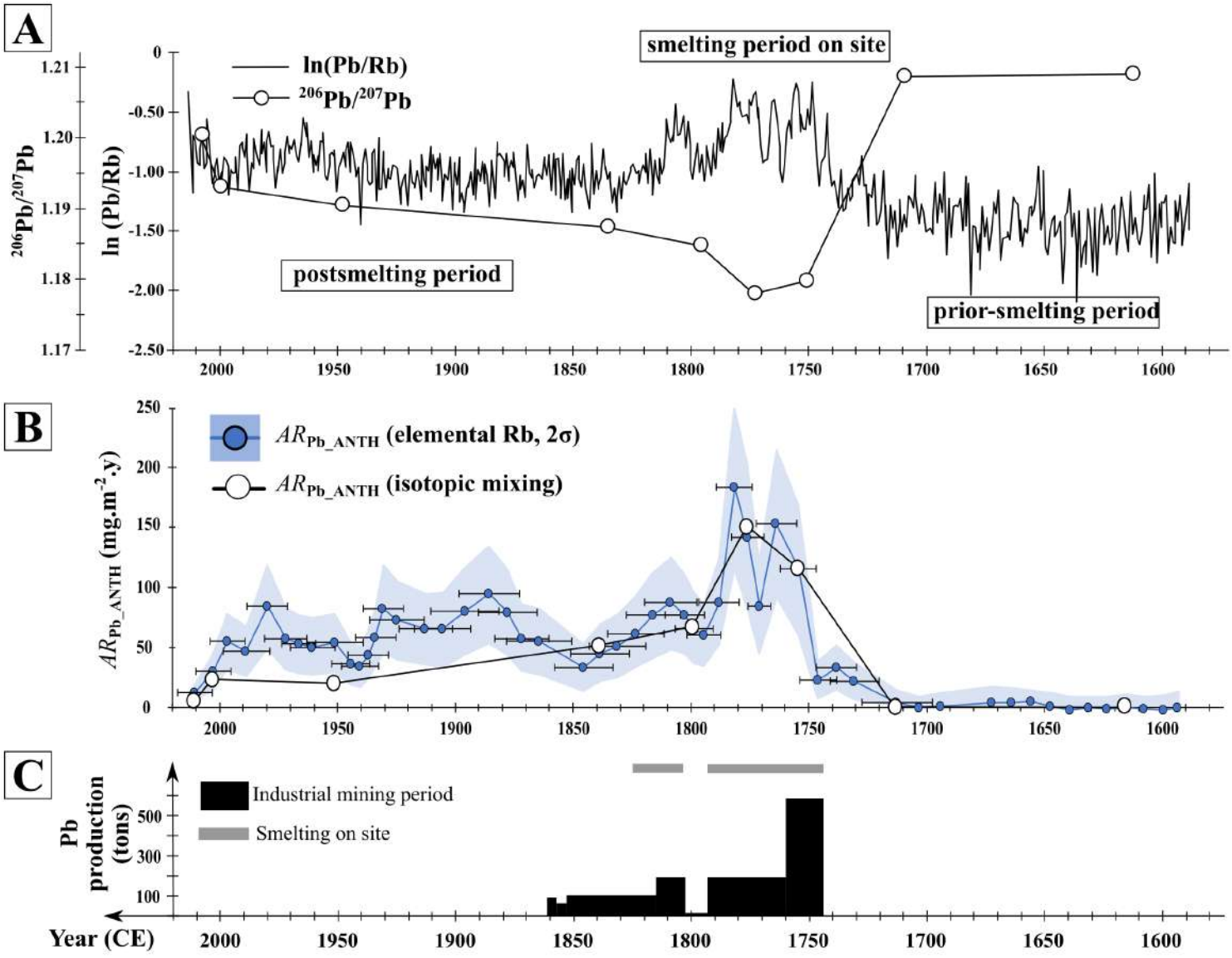

Figure 7: A) The ratio ln(Pb/Rb) from EDS-XRF data according to time (age CE) divided into 3 periods : pre-smelting, smelting and post-smelting periods with $^{206}Pb/^{207}Pb$ ratios of 9 samples along PLG-03; B) Accumulation rate of anthropogenic Pb (AR_{Pb_ANTH}) calculated using both the elemental ratio (Rb) and Pb isotopes (equations 2 and 3); C) Historical timeline of the ore production from 1745 to 1865 yr cal CE.

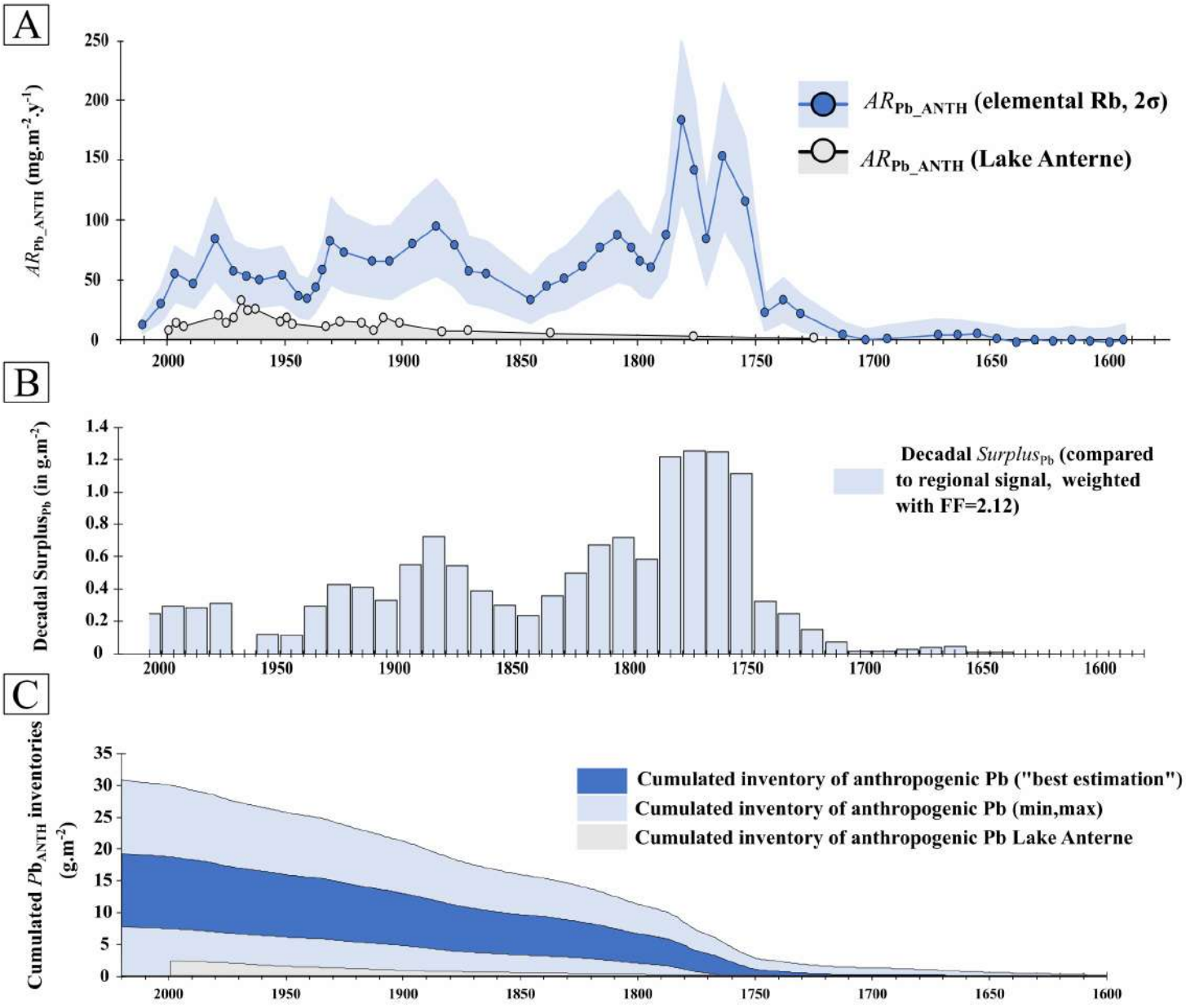

Figure 8: Comparison between Lake La Plagne and Lake Anterne. A) Comparison between AR_{Pb_ANTH} of Lake Anterne and of Lake Plagne; B) Local surplus of Pb_{ANTH} per m^2 calculated from AR_{Pb_ANTH} subtracted from the regional signal (2.12 x Lake Anterne); C) Cumulated Pb_{ANTH} through time in both lakes corresponding which in turn correspond to the total inventory recorded in lakes at the sampling date.